ULTRA-LINEAR POLYMER MODULATOR

Lumera Corporation

APPROVED FOR PUBLIC RELEASE; DISTRIBUTION UNLIMITED.

AIR FORCE RESEARCH LABORATORY
SENSORS DIRECTORATE
ROME RESEARCH SITE
ROME, NEW YORK

STINFO FINAL REPORT

This report has been reviewed by the Air Force Research Laboratory, Information Directorate, Public Affairs Office (IFOIPA) and is releasable to the National Technical Information Service (NTIS). At NTIS it will be releasable to the general public, including foreign nations.

AFRL-SN-RS-TR-2006-154 has been reviewed and is approved for publication

APPROVED: /s/

                    BRIAN F. MCKEON
                    Project Engineer

FOR THE DIRECTOR: /s/

                    RICHARD G. SHAUGHNESSY
                    Chief, Rome Operations Office
                    Sensors Directorate

REPORT DOCUMENTATION PAGE

Form Approved
OMB No. 074-0188

Public reporting burden for this collection of information is estimated to average 1 hour per response, including the time for reviewing instructions, searching existing data sources, gathering and maintaining the data needed, and completing and reviewing this collection of information. Send comments regarding this burden estimate or any other aspect of this collection of information, including suggestions for reducing this burden to Washington Headquarters Services, Directorate for Information Operations and Reports, 1215 Jefferson Davis Highway, Suite 1204, Arlington, VA 22202-4302, and to the Office of Management and Budget, Paperwork Reduction Project (0704-0188), Washington, DC 20503

1. AGENCY USE ONLY (Leave blank)	2. REPORT DATE MAY 2005	3. REPORT TYPE AND DATES COVERED Final Aug 03 – Nov 05

4. TITLE AND SUBTITLE ULTRA-LINEAR POLYMER MODULATOR	5. FUNDING NUMBERS C - F30602-03-C-0119 PE - 62500F PR - 517D TA - SN WU - 02
6. AUTHOR(S) Lou Bintz, Alan Mickelson	

7. PERFORMING ORGANIZATION NAME(S) AND ADDRESS(ES) Lumera Corporation 19910 North Creek Parkway Bothell Washington 98011-6540	8. PERFORMING ORGANIZATION REPORT NUMBER N/A

9. SPONSORING / MONITORING AGENCY NAME(S) AND ADDRESS(ES) Air Force Research Laboratory/SNDP 25 Electronic Parkway Rome New York 13441-4515	10. SPONSORING / MONITORING AGENCY REPORT NUMBER AFRL-SN-RS-TR-2006-154

11. SUPPLEMENTARY NOTES

AFRL Project Engineer: Brian F. McKeon/SNDP/(315) 330-7348 Brian.McKeon@rl.af.mil

12a. DISTRIBUTION / AVAILABILITY STATEMENT APPROVED FOR PUBLIC RELEASE; DISTRIBUTION UNLIMITED.	12b. DISTRIBUTION CODE

13. ABSTRACT *(Maximum 200 Words)*

Polymer electro-optic modulators with applications to photonic link systems requiring high spur free dynamic range are discussed. Multilayer high $\mu\beta$ electro-optic polymer modulators were designed, fabricated and tested. The linearized designs include three-electrode electro-optic modulators, 3dB coupled directional couplers, Mach Zehnder modulators, dual drive modulators. The problem of bias drift is thoroughly discussed. A 3dB coupled directional coupler with increasing separation between arms (splayed) was modeled, fabricated and tested as a candidate for a bias free modulator.

14. SUBJECT TERMS Electro-Optic Modulator, Photonic Link, Chromophore, Spur Free Dynamic Range, Directional Coupler, Mach Zehnder, Linearized Modulator, Fiber Optic, Bias Drift	15. NUMBER OF PAGES 69
	16. PRICE CODE

17. SECURITY CLASSIFICATION OF REPORT UNCLASSIFIED	18. SECURITY CLASSIFICATION OF THIS PAGE UNCLASSIFIED	19. SECURITY CLASSIFICATION OF ABSTRACT UNCLASSIFIED	20. LIMITATION OF ABSTRACT UL

NSN 7540-01-280-5500

Standard Form 298 (Rev. 2-89)
Prescribed by ANSI Std. Z39-18
298-102

Table of Contents

List of Figures

1.0 Introduction and Summary Results:

Polymer electro-optic modulators with applications to photonic link systems requiring high spur free dynamic range (SFDR) are discussed. Examples of design, fabrication and test results are presented. Triangle wave optical response of linearized polymer modulators in the quasi-small signal photonic link domain is graphically depicted and the multilayer polymer waveguide structure is described

Electro-optic modulators capable of high speed operation that possess a highly linear electrical to optical transfer function and retain reasonable optical transparency are potential enablers for optically addressed phased array radar applications. Based on state of the art Lumera polymer electro-optic modulators, an ultra-linear polymer modulator program was carried out over a two year period. The design for ultra-linear electro-optic response was focused on two major design paradigms: a pre- and post-biased 3/4 coupling length directional coupler design, and a 3dB coupled directional coupler design. To quantity the transference of theoretical designs into polymer devices, passive polymer core waveguide structures, e.g. straight waveguides, directional couplers and waveguide splitters were fabricated and tested in parallel with the RF electro-optic devices. These passive waveguide devices quantified the required waveguide coupling in the directional coupler devices and assured the polymer electro-optic Mach-Zehnder devices were operating in the single mode regime. Polymer electro-optic modulators were fabricated in Lumera's clean room facility, diced and tested at Lumera and the University of Colorado at Boulder. These polymer electro-optic modulators were quasi-trench designs utilizing low index polymer claddings and guest-host electro-optic polymer core materials with high $\mu\beta$ Lumera synthesized chromophores.

The ultra linear design, a 3-electrode directional coupler modulator, was fabricated utilizing the same three layer polymer quasi-trench waveguide. These polymer ultra-linear modulators show excellent qualitative linearity in the small signal regime when driven by a triangle waveform electrical feed.

Ultra Linear Directional Coupler
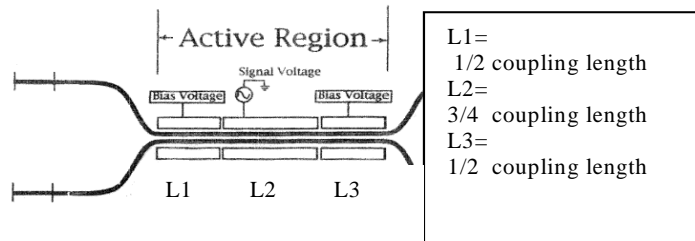
Figure 1: Three-Electrode Directional Coupler

Mathematical modeling of the optical power modulation as a function of the radio frequency (RF) driving voltage of such a three-electrode directional coupler is shown below. For high spur free dynamic range (SFDR) applications the transfer function of interest is a small signal regime centered on the region where the applied voltage to the electro-optic polymer is zero.
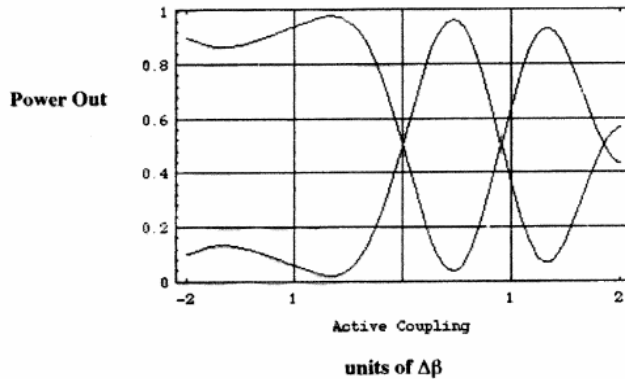
Figure 2: Predicted transfer function for two bias electrodes of length approximately equal to one half of a passive coupling length and a central signal electrode of approximately 3/4 of a complete passive coupling length

Polymer three-electrode directional couplers were fabricated and driven in the lab under small signal conditions with a triangle waveform. In the following Labview™ screen capture the driving electrical field is plotted along with the optical signal observed at the free space detector:
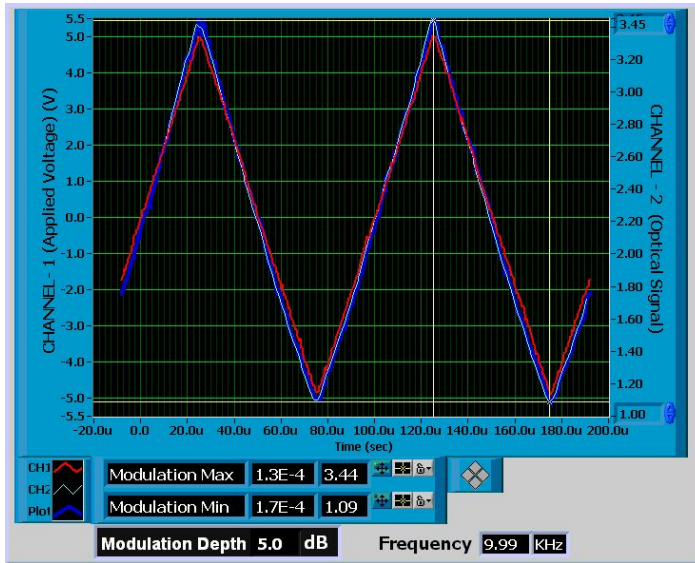
Figure 3: Small signal e-o response of three electrode directional Coupler

A new and novel design was also fabricated during this project: a 3dB coupled splayed electro-optic polymer directional coupler modulator. This modulator also showed excellent small signal electro-optic response to a triangle wave electrical signal. Shown below is a composite graphical montage of the various salient features of this modulator design: waveguide layout, the predicted SFDR, and optical test results:
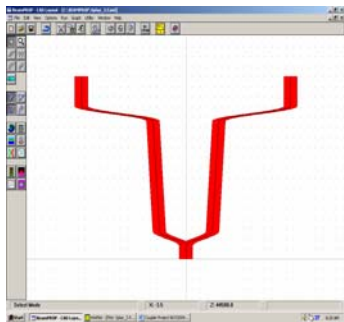
Figure 4: Splayed 3 dB coupled directional Coupler Modulator
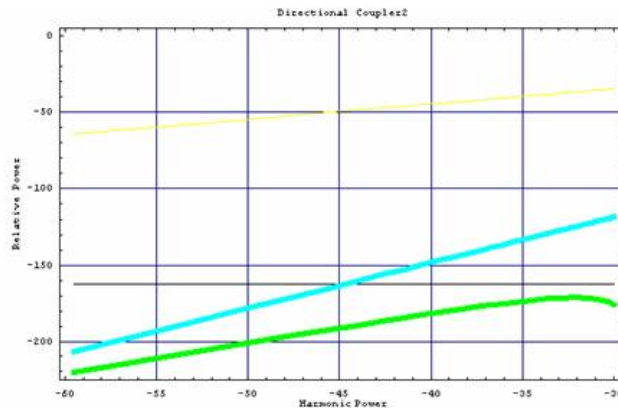
Figure 5: SFDR simulations of a splayed 3 dB coupled directional coupler: Signal (yellow) Second Harmonic over tone (Green) Third Harmonic (BLUE) Noise Floor (BLACK)

3
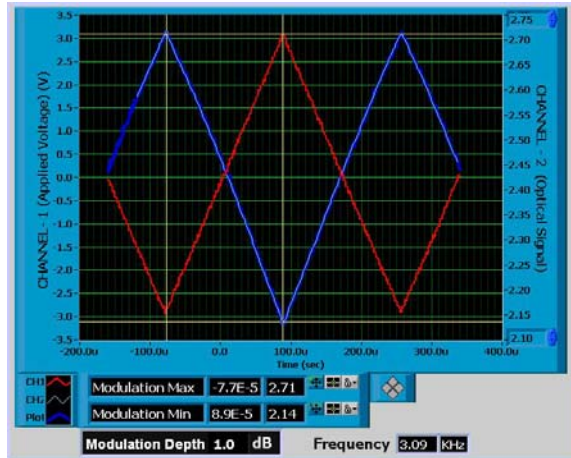
Figure 6: small signal e-o response of a 3 dB coupled splayed directional coupler

To our knowledge this is the first electro-optic 3 dB coupled splayed directional coupler to be designed, fabricated and optically tested. The results are encouraging and future directions in polymer ultra-linear modulator design, fabrication and testing are presented in the concluding remarks.

2.0 Photonic Design and Polymer Modulator Fabrication

Multilayer high μβ electro-optic polymer modulators were fabricated and tested. The linearized designs included three-electrode electro-optic modulators, 3 dB coupled directional couplers, splayed 3dB directional couplers, Mach Zehnder modulators, dual drive modulators, splitter coupled splayed directional coupler, passive directional couplers and straight waveguides. The polymer electro-optic modulator results and discussions are broken down into the following sections: **2.1** Single-electrode directional coupler with DC bias; **2.1.1** Fabrication and modeling passive polymer directional couplers for single mode operation; **2.1.2** Fabrication and modeling single-electrode directional couplers **2.1.3** Design Directional Coupler test structures and optical modulators: Multi-section Directional Coupler modulators;

2.2 New Advanced Modulator Designs: Splayed 3dB coupled Directional Coupler

2.2.1 Lot 260: Splayed Directional Couplers and optical loss of 22% DH6/APC vs 27% DH6/APC polymer core **2.3.** Lot X200-3, X237-21: Active three-electrode directional coupler results:

2.1.3.1.1 Design high frequency electrode structures for radio frequency (RF) modulation of light

Two-tone third-order inter-modulation distortion in integrated optic amplitude modulators has been extensively studied in the literature, through techniques that include polarization-mixing, dual parallel modulators, and modified directional coupler modulators [1, 2].

Directional coupler modulators are devices in which the optical eigenmodes of the modulating structure have a distributed coupling coefficient over the entire length of the device. By using multiple electrodes, increased linearity of the directional coupler transfer function is accomplished through manipulation of the optical eigenmodes of this two waveguide system. The linearized directional coupler with a pre-bias active section and a post-bias active section seems among the most tunable schemes for high frequency, linear modulator operation.

2.1 Single electrode directional coupler with DC bias

The device functionality of any given section of the multi-section modulator is based on an electro-optic DC biased single-electrode directional coupler. The expected SFDR of the ultra-linear transfer characteristic of a single electrode DC biased directional couplers is ~100 dB [2].
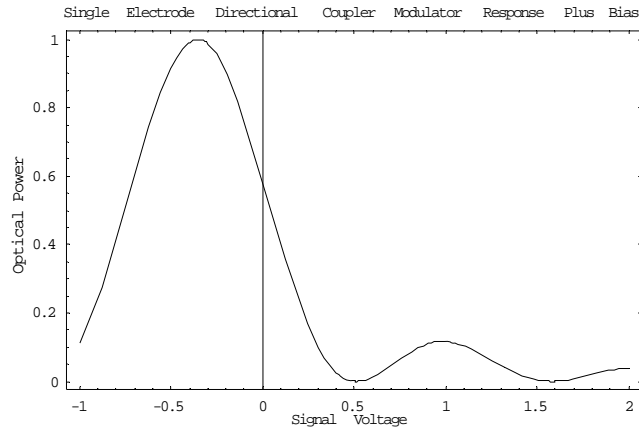
Figure 7: Optical power versus applied voltage for a directional coupler with single electrode with DC bias. The signal voltage is scaled in units of Vpi.

2.1.1 Fabrication and modeling passive polymer directional couplers for single mode operation in the near I.R.

Underpinning all polymer waveguide fabrication is multi-layer spin coating and curing of optically transparent polymers. Polymer thickness and refractive index control of these polymers allows design of single mode vertical confinement. The refractive index of the APC/DH6 core material was ~1.62 @1550nm and the optical polymer cladding material had a refractive index of ~1.50. The bottom and top clad were ~3.0 μm in thickness and the core material was spin coated to ~2.7 μm thickness. In this high Δn core/clad system, horizontal modal confinement is created by utilizing a DRIE reactive ion etching process to define a relatively shallow ~0.8 μm deep trench in the bottom clad prior to the core spin coating and curing process. This quasi-trench design is robust to index fluctuations of various core/clad combinations but realization of less than 3 dB loss in the optical coupling to the input and output optical fibers requires usage of a high N.A. specialty optical fiber.

The initial fabrication and design simulations were targeted to quantify the coupling between adjacent waveguides in the directional coupler. To accomplish this, one test cell on the waveguide layer photo-litho mask was designed with an array of directional couplers.

The mask design for baseline devices used the following BeamProp™ model to determine the appropriate center-to-center waveguide separation distance for multi-layer polymer couplers with a 2.3 cm long active length:
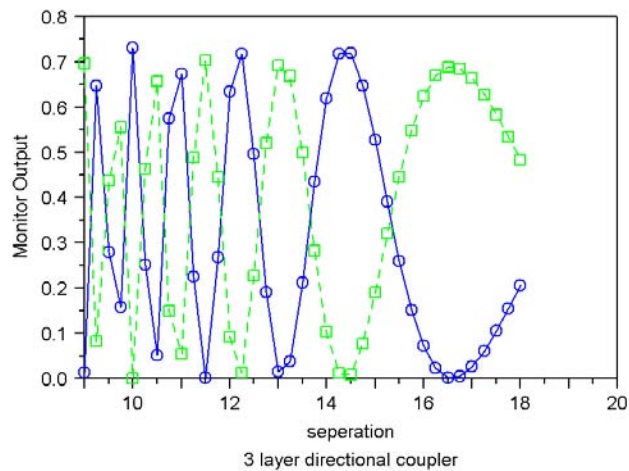
Figure 8: Output Intensity vs. waveguide separation for a 2.3 cm nominal length directional coupler in a three layer quasi-trench structure

From these simulations we set the nominal waveguide separation to 16.7 µm center to center. BeamProp™ was also used for the lithographic waveguide layer mask layout. Figure 9 illustrates two test directional couplers that were incorporated into the test cell.
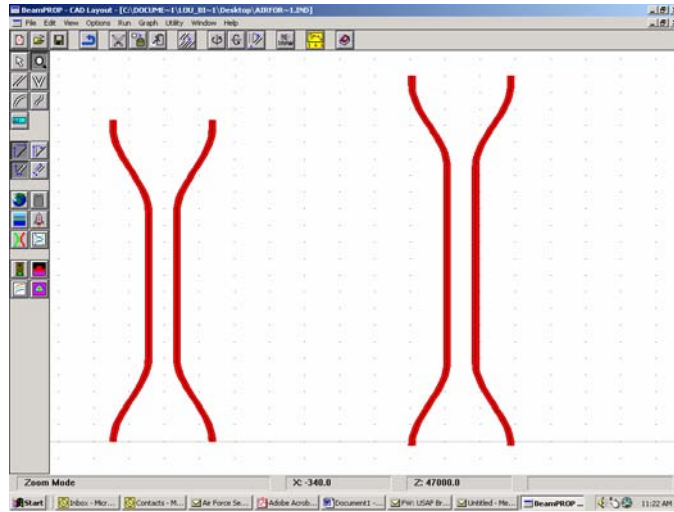
Figure 9: Passive Directional Coupler Test Structures, ¾ coupling length directional coupler and one-coupling length directional coupler

In figure 9, the longer directional coupler is a one-coupling length polymer directional coupler and the shorter coupler is a ¾ coupling length directional coupler. This structure is the same as the center signal section of a three-electrode ultralinear directional coupler. These couplers were modeled in BeamProp™ and the simulations predicted the 1550nm optical coupling properties.
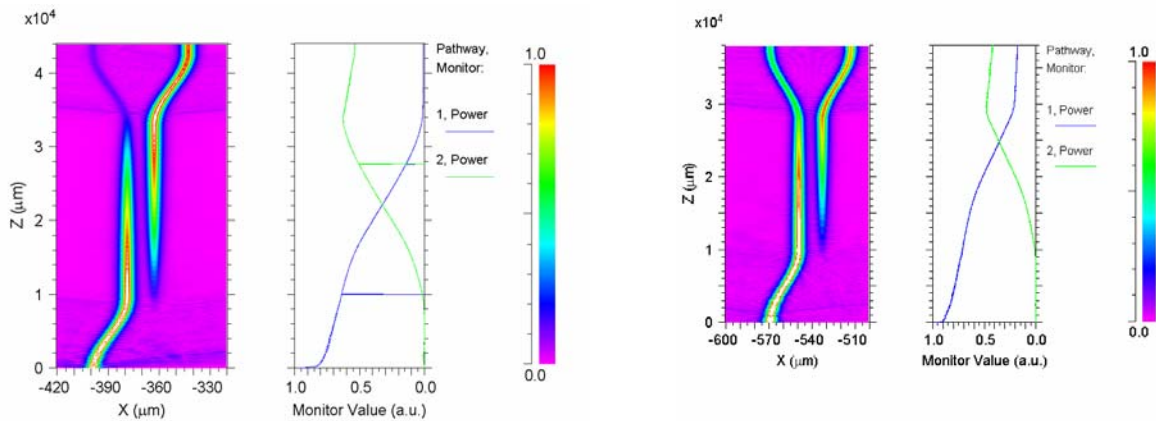
Figure 10 & 11: One-coupling length polymer directional coupler simulation (left) ¾ coupling length polymer directional coupler(right)

Passive three layer polymer waveguides were fabricated and tested for design verification. Figure 12 shows the optical mode false color capture data for Lumera lot 160-7 on ¾ length directional coupler.
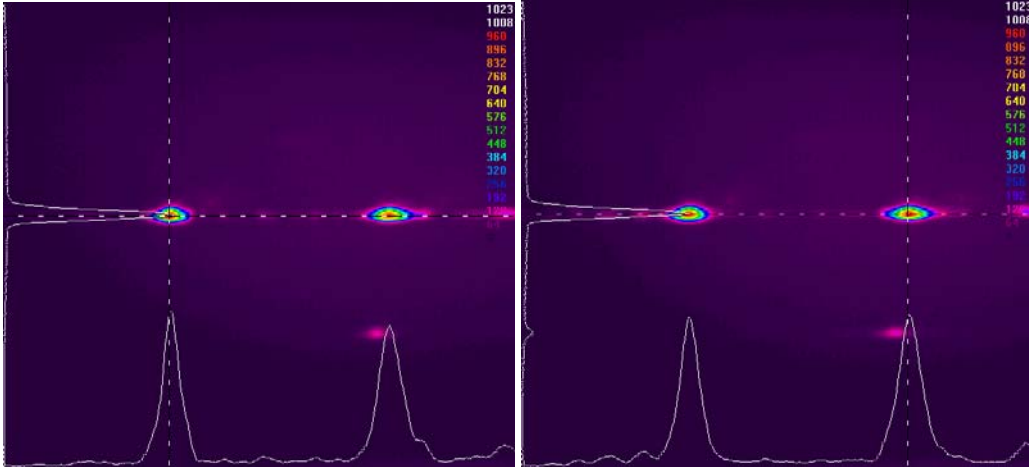
Test results: 160-7
L5 Chip Directional Coupler # 2

Figure12a: These results show 50:50 splitting on a predicted 3/4 coupling length directional coupler.
(above, right)
Figure12b: Optical input port is switched from one arm of the directional coupler to the other arm
(above, left)
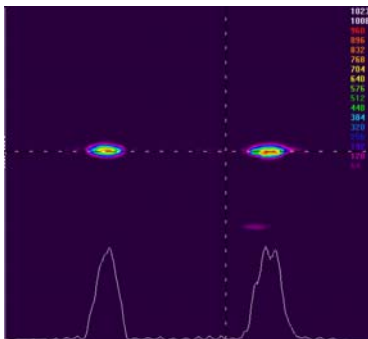
Figure 13: Additional fabrication runs focused on confirming and selecting the proper stack for proper
passive waveguide coupling.

For example here are the test results for a ¾ coupling length directional coupler from lot X186-6: the expected outcome from a ¾ length directional coupler would be a 50:50 optical splitting at the output. Optical testing verified the 3dB splitting on these passive directional couplers. This milestone confirmed a well controlled fabrication process

Passive three layer polymer waveguides were fabricated and tested for design verification. These polymer optical devices performed the mode splitting and coupling fashion in a way that was reproducible and closely matched the optical models simulated with the BeamProp™ software. Thus the critical processing control of polymer waveguide fabrication, paramount to creating working polymer modulators, was clearly demonstrated. Once this milestone was met, work proceeded on to designing and fabricating active polymer modulators.

2.1.2 Fabricate and model single electrode directional couplers

   Ultra-linear modulators and standard high speed Mach Zehnder and directional couplers were designed, masked and fabricated at Lumera utilizing amorphous polycarbonate polymer/high μβ electro-optic chromophore guest/host polymer core with cross-linkable polymer claddings. These polymer modulators were fabricated on 6-inch high resistivity Si substrates in Lumera Corporation clean room facility. In addition to the cladding and core deposition, waveguide definition, dicing and other processes required for the fabrication of passive polymer waveguides, two critical processing steps are required for the fabrication of electro-optic polymer modulators: high electric field poling of the electro-optic core at elevated temperatures slightly above the glass transition temperature of the polymer core material and the formation of the poling and drive electrodes required for high speed RF operation. The criticality of the poling process is driven by the competing requirements of keeping the glass transition polymer conductivity minimal and simultaneously allowing rotation of the chromophore to align parallel with the applied external field while being buffeted by randomizing effects of kT induced phonon vibrations of the polymer host. Additionally, the requirement to drop a large field across the core, 80- 120 V/μm, requires the uniformity, relative permittivities and conductivities of the core/clad polymer stack,(at the poling temperature used during the poling process), be such that most of the field is dropped across the core and not induce dielectric breakdown in any of the polymer layers. Flatness and uniformity of the gold electrodes is also critical since spikes in the bottom gold layer will lead to electric field concentration and induced dielectric breakdown of poling current during the poling process.

        Measured Vpi for a given polymer modulator with a known total stack height and electrode length directly yields the effective r_{33} of the polymer core material. Three μm thick electro-optic core polymer spun onto ITO glass substrates consistently show higher r_{33}, as measured by single layer Teng Mann measurement techniques, than the r_{33} currently producible

in low optical loss polymer Mach-Zehnder modulators. This difference may be due to the complexities of poling a multi-layer polymer partially conducting stack, the balancing of optical loss induced in poly-carbonate APC/DH6 electro-optic core material vs. Vpi, or some other condition creating lower measured waveguide electro-optic coefficients.

The acentric ordering of the chromophore via the high temperature poling process results in an electro-optic coefficient that, in the weak field approximation, is proportional to the number density of the chromophore, to the electric field applied to the chromophore, and to the second order hyperpolarizability of the chromophore times the dipole moment. During the poling process this ordering effect is counteracted by 5kT, where K is Boltzmann's constant and T is the poling temperature in degrees Kelvin. Extending a weak field approximation[1] to a multi-layer polymer waveguide stack with temperature dependent conductivities and dielectric constants, at some steady state the expected r_{33} can be written as:

---

[1] Gunter et.al. Organic Nonlinear Optical Materials 1995 Vol.1

$$r_{33} = 2N\beta_{zzz}\left(\frac{\varepsilon(T)\left(n^2+2\right)^2}{3n^2\left(n^2+2\varepsilon(T)\right)}\right)^2 \frac{\mu_{chromphore}E(T)_{Poling\_across\_core}}{5KT}$$

There are time dependent phenomena in the poling process, such as ramping to the ~Tg poling temperature and applying the voltage to the stack. Correct analysis would require a time–dependent model; however many additional parameters such as the strength of local polymer "viscous" friction would then need to be included. Additionally, the poling temperature is in the neighborhood of the glass-rubber transition of the host polymer; the conductivity and the permittivity of the APC/DH6 guest-host electro-optic polymer core are varying rapidly in the temperature regime. Gaining insight into the "best" poling profile, i.e. one which gives the same r_{33} value as single layer poled e-o polymer films without poling induced optical loss, is quite difficult and currently an experimental affair. Empirical modeling of such polymer phenomena may be the best way to gain additional insight into the poling process.

We measured the individual thin polymer layer conductivity and permittivity values and tried to maximize the electric field drop across the polymer core, thereby minimizing the drop across the polymer bottom and top cladding layers. For the materials used on this program we recorded the following conductivity and poling currents and voltage poling profiles.
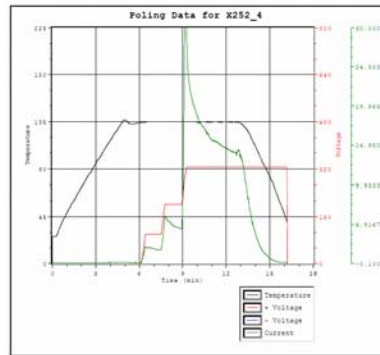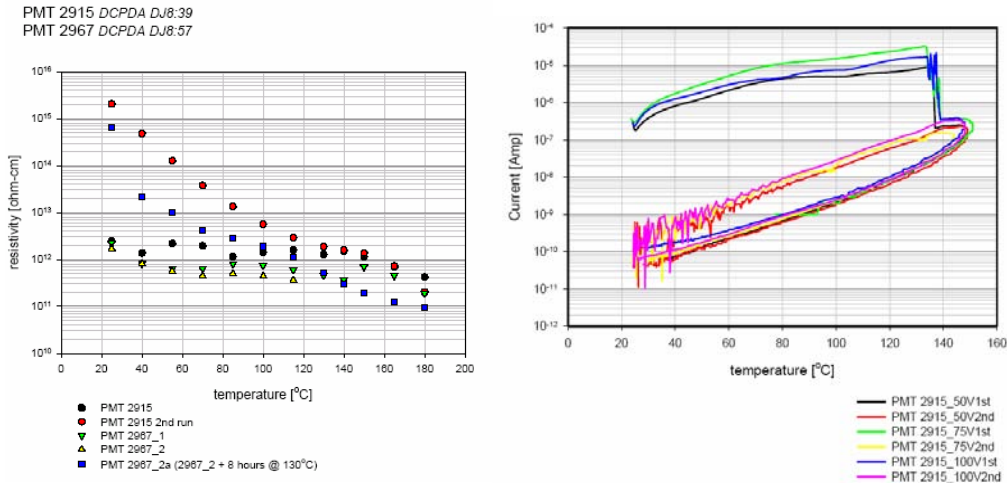
Figure 14, 15, 16: Thin Film Poling Conductivity vs temperature/voltage

Black is temperature, green is current through the stack, red is voltage applied.

- Lumera polymer claddings:
    - V60 bottom clad (uv crosslinkable acrylate)
    - V82 bottom clad (uv crosslinkable arcrylate)
    - MG13 bottom clad(thermal crosslinkable siloxane)
    - P9 Top Clad   (uv crosslinkable acrylate)

Triple stack poling data from recent studies of various layers in the polymer stack:

Particularly interesting is the poling current time dependencies.

V60 acrylate :
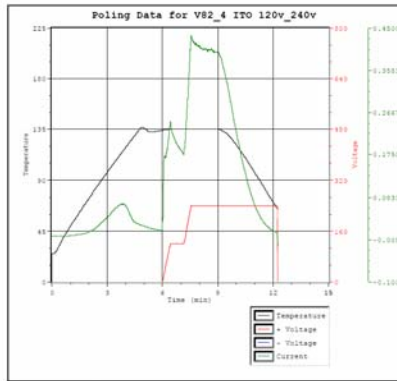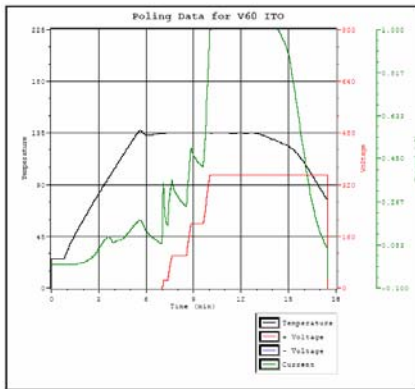
Figure 17, 18: Thin Film Lumera Clad Conductivity vs. temperature/voltage

V82 acrylate:
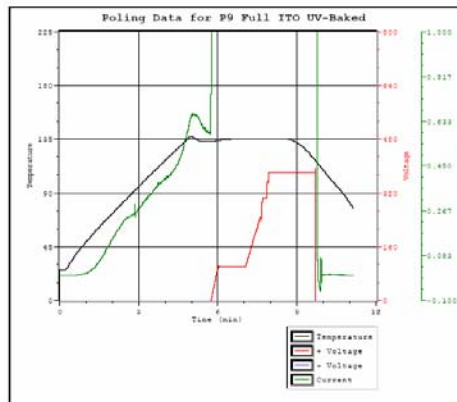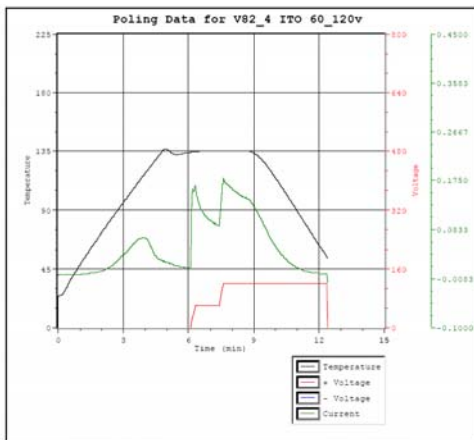
Figure 19, 20: Thin Film Lumera P9 Top Clad Conductivity vs. temperature/voltage

All electro-optic core materials for this program were amorphous poly-carbonate in guest/host combination with Lumera synthesized high $\mu\beta$ chromophore DH-6. Optical loss at 1550nm due to chromophore absorption is mitigated by maintaining the maximum absorption peak of the chromophore to below 750 nm. The SCI optical metrology tool can verify lambda max of the electro-optic chromophore in thin films as well as the index of refraction and dispersion for all the polymer layers in a waveguide stack. Below is the chemical composition of DH6, a ring

locked tricyano-furan acceptor based electro-optic chromophore and the SCI index of refraction and absorption spectra:
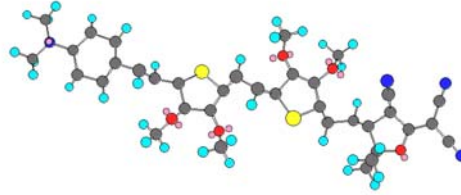
Figure 21: Lumera DH-6 Chromophore

The refractive index and absorption as measured on a 2 μm thin film is shown below. This data was taken with a SCI4000 thin film spectroscopic tool.
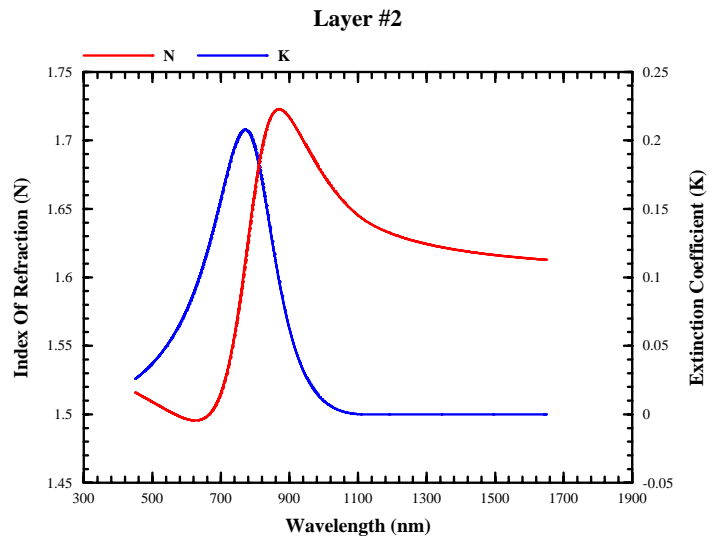
Figure 22: DH6/APC Kramers –Koenig Curves
1st Clad Layer Thickness = 2305.95 nm

Critical to proper poling of the core is quantitative conductivity and Tg measurements. Electro-optic core DH6/APC was measured in thin films of 3 μm thickness and the temperature dependence of the conductivity was measured.
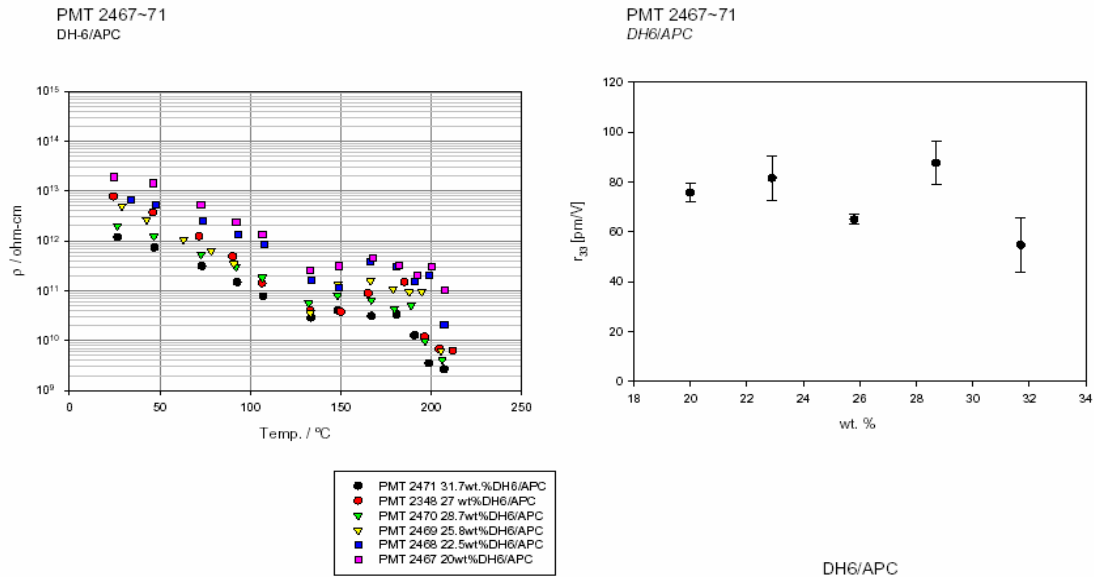
Figure 23, 24: DH6/APC conductivity vs temperature for various chromophore concentrations

Key Lumera three layer polymer waveguide stack features and optical waveguide performance characteristics are shown:

Figure 25, 26 top: SEM Three Layer Quasi-trench polymer waveguide
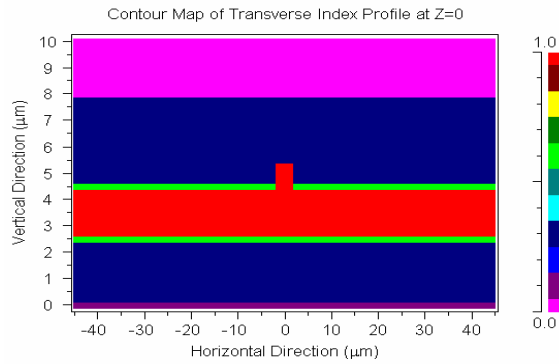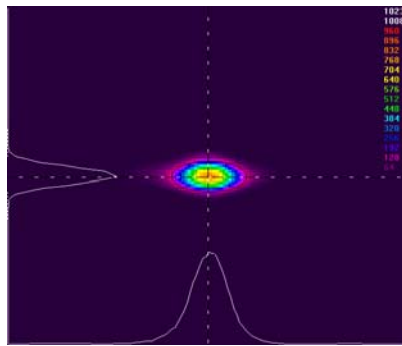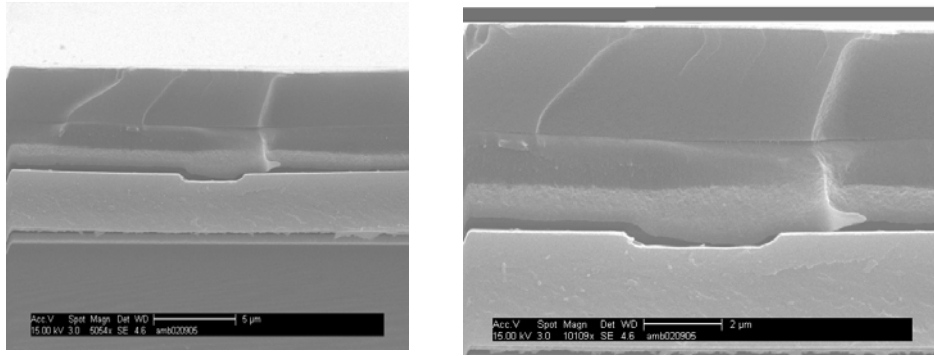
Figure 27: Beam-Prop Simulation of Polymer Stack   *Figure 28: Beam Prop polymer stack simulation*

Fimmwave Laplace Solver:

Prediction of Voltage Drop across the core during poling
Waveguide stack is a three layer high Δn system with a symmetric $\varepsilon = 4$ top/bottom cladding and a DH6/APC electro-optic core. We have successfully modeled the waveguide mode and the Laplace field solver shows the predicted field across the core layer.
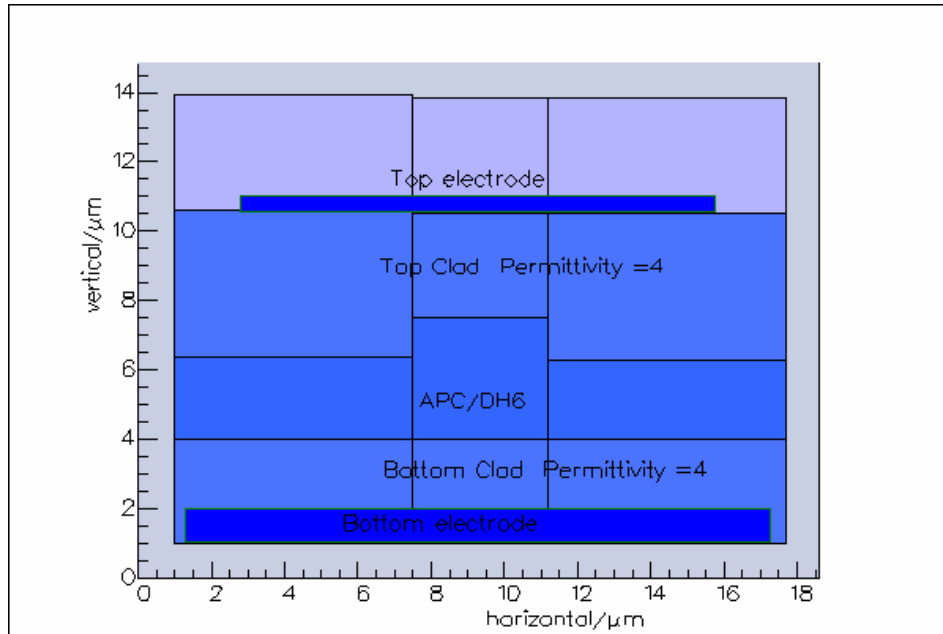
Figure 29: Modeled polymer waveguide cross section

The polymer stack consists of a top and bottom clad with a permittivity = 4 and an APC/DH6 electro-optic core. The current model uses the room temperature permittivity of the core. Current 2-D Laplace solver code can generate the electric field across the core if the layers are insulating and also generate the optical mode profile.
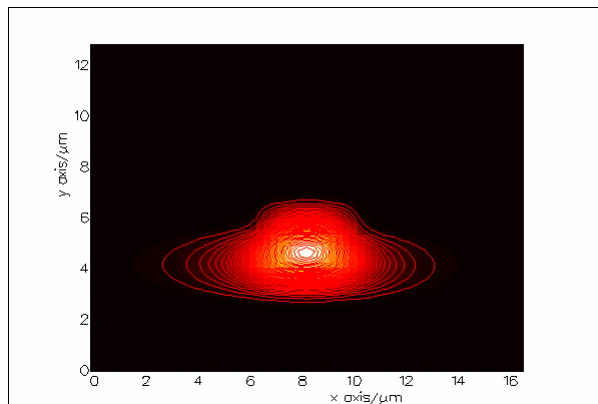
Figure 30: Optical mode cross section (intensity)
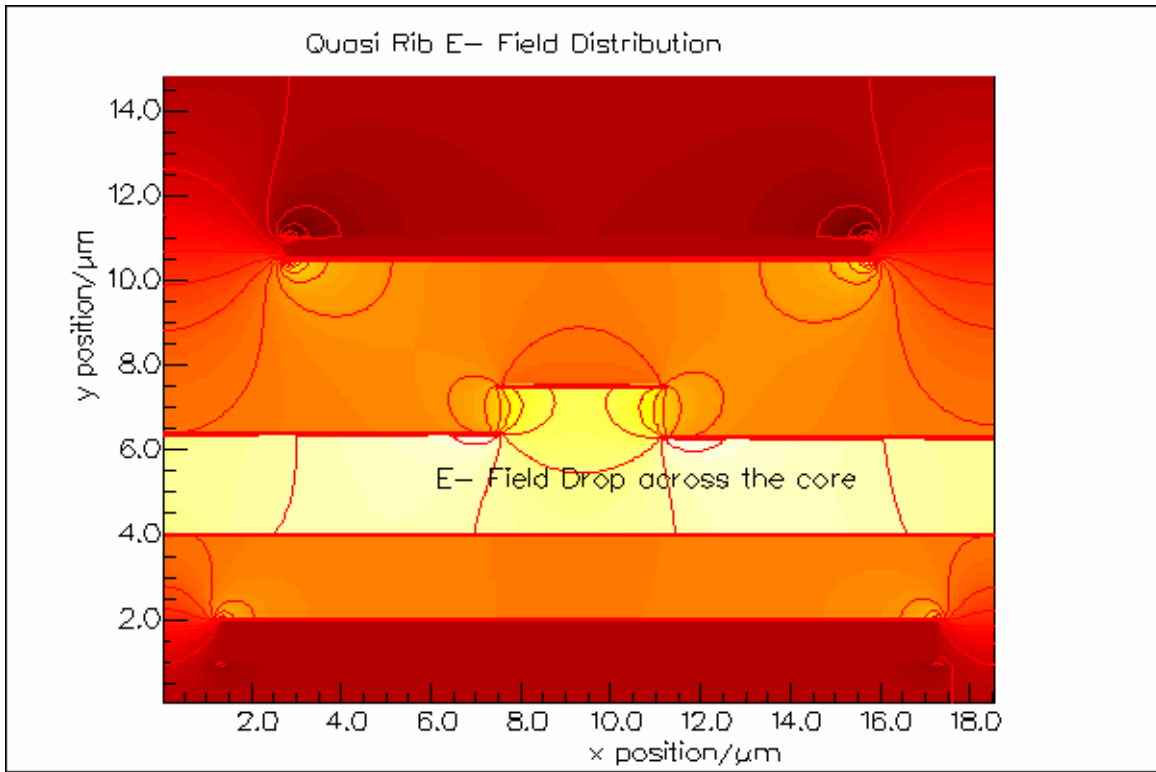
Figure 31: False Color E-field calculation in polymer waveguide stack: 600V applied

A 3-D view of the E-Field across this waveguide stack at 600V applied poling voltage is shown below:
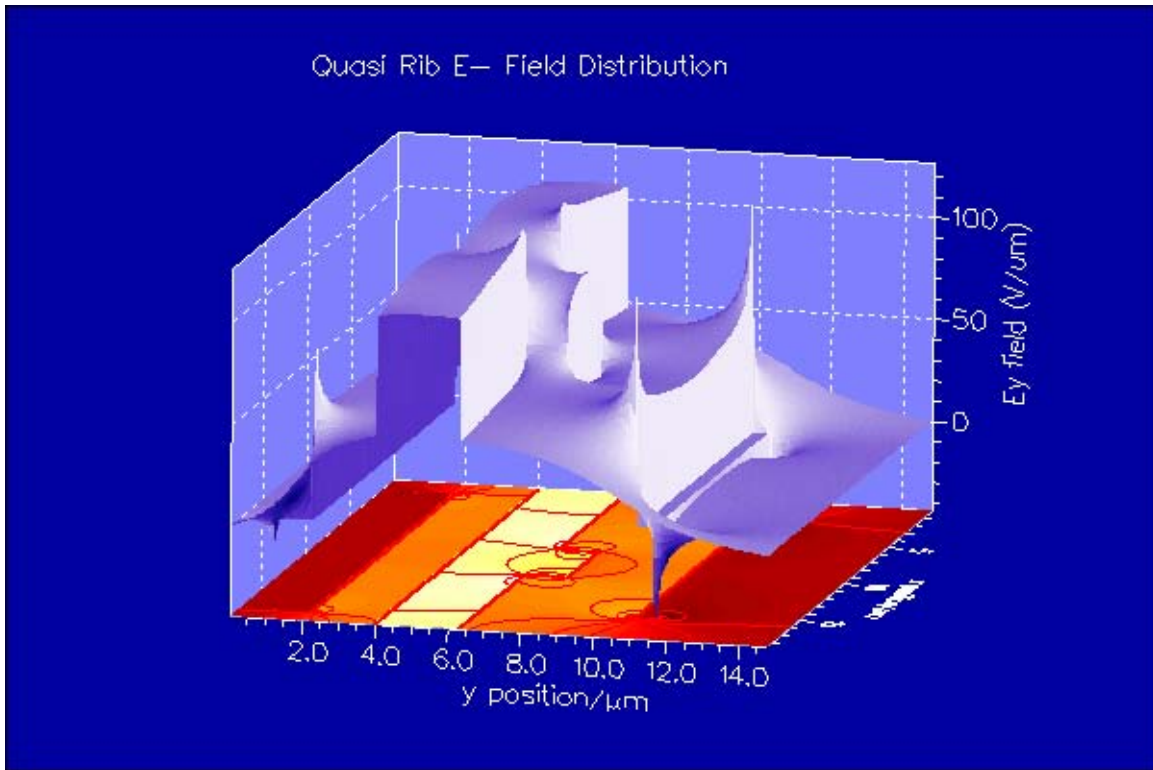
Figure 32: 3-D view of Ey Field: 80-105 V/μm across core with 600V applied
In this waveguide polymer stack model. The field across the core is ~105V/μm in the
non-trench area and ~85 V/μm in the waveguide trench area. Note the edge singularities
are also approaching 100 V/μm.

Lumera processes on a six-inch wafer fabrication facility. Each wafer contains approximately 60
cells. The large number of polymer electro-optic devices provides the opportunity to measure full
wafers for statistical verification of Vpi, optical loss etc. In the next section the fabrication runs
done to experimentally verify the optical performance of various modulator designs is presented.
Optical testing was performed at Lumera using an optical test bench configured as shown below:
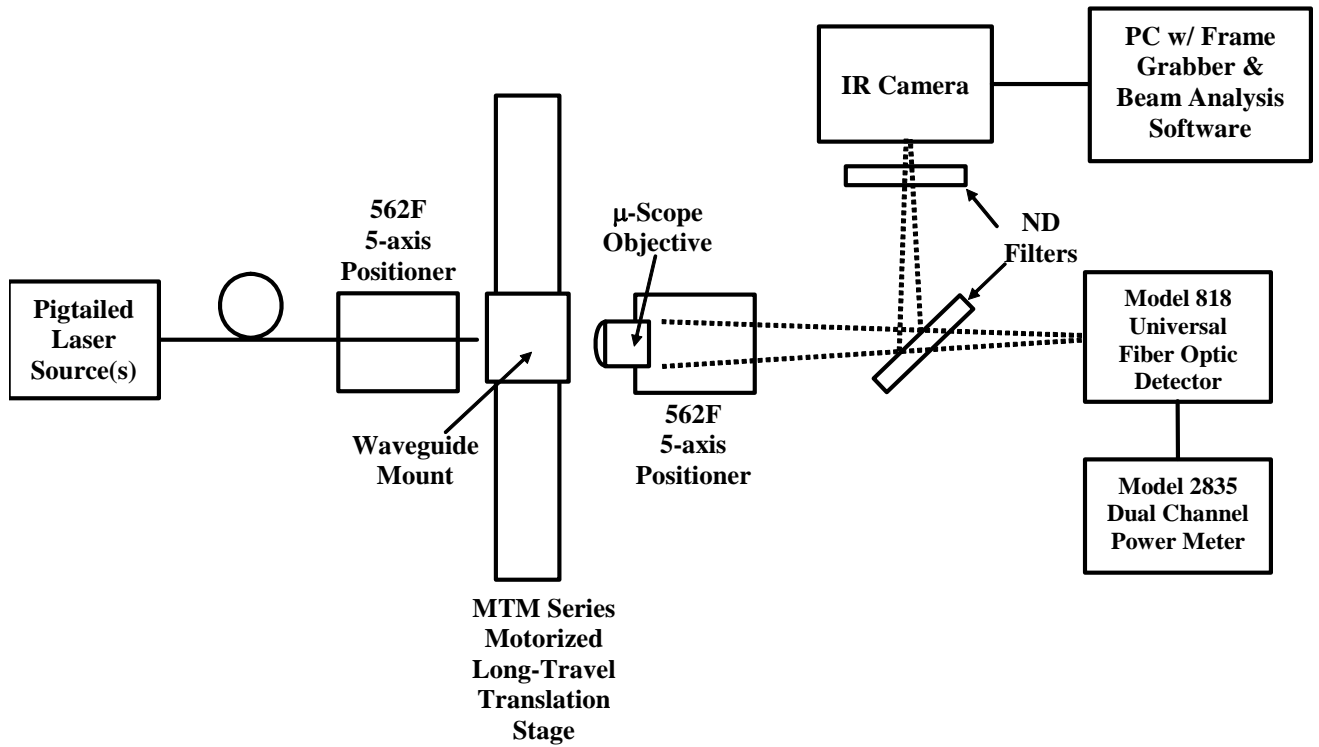
Figure 33:   optical test bed: lumera

Since Lumera currently has no capacity for SFDR testing. An effort was started at the University of Colorado at Boulder to extend our test capacity and initial optical and RF results are presented in Appendix B. The basic configuration of the U.C. Boulder test bed is shown below:

SFDR Testing:
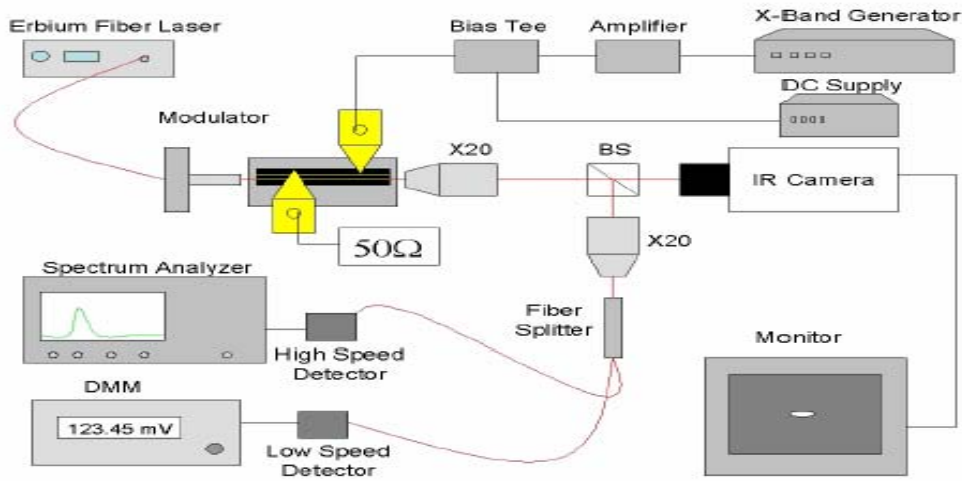
Figure 1: Picture of the setup used to measure the modulator parameters.

Figure 34: U.C. Boulder SFDR Test bed; Early results were limited by the optical loss of the polymer modulator and fiber coupling mechanisms used during the SFDR testing process

In order to baseline and to confirm the operational characteristics of the polymer modulators being fabricated lot X254-19 was fabricated and Mach-Zehnder modulators were measured across the surface of the die. Below is a table of the recorded optical loss and low frequency Vpi measurements done on this wafer.

Lot X254-19:

Wafer level Study of the optical loss vs. Vpi on single arm drive Mach Zehnder structures across the wafer

Wafer X254_19	Chip	Loss free-s	Loss fiber-	Loss bias	V-pi	Extinction
X254_19	A1	-13.7	-17.5		4.8	17.5
X254_19	A2	-12.2	-15.6		5.3	23.7
X254_19	A3	-13.1	-15.1		5.5	23.2
X254_19	A4	-12.8	-14.8		5.6	21.2
X254_19	A5	-11.8	-14.2		4.8	26.7
X254_19	A7	-13.1	-16.2		5.3	28.9
X254_19	A8	-13.3	-15.6		5.3	27
X254_19	A9	-12.5	-14.4		5.3	24.9
X254_19	A13	-12.5	-14.4		5.3	20
X254_19	A14	-12.5	-15.6		5.2	20.6
X254_19	A15	-11.9	-14.1		5.5	20.4
X254_19	A16	-11.9	-14.2		5	21.2
X254_19	A12	-12.4	-14.3		5.5	17.3
X254_19	A6	-11.7	-13.9		5.3	34.2
X254_19	A10	-15				
X254_19	B3	-12.1	-15.2		5.2	30.4
X254_19	A5	-14.2	-16.3		5.3	26.3
X254_19	A14	-14.3	-16.4		5	24.7

Figure 35: Vpi and optical loss across a full wafer with an applied full wafer contact poling scheme

Uniformity of the Vpi across the wafer and the optical loss variance was excellent. This wafer was processed utilizing a full wafer contact poling scheme. The consistency shows that multiple optical designs can be tested and compared on a given wafer and device performance can be expected to be reasonable correlated to the design modeled in the various software packages. In Appendix A the criticality of optical loss and the impact of Vpi on SFDR is mathematically analyzed.

2.1.3 Design Directional Coupler test structures and optical modulators:

Multi-section Directional Coupler modulators

To exceed a 120 dB spur free dynamic range, mathematical analysis was performed to determine the direction and focus of extending the linearity of these high E.O. polymer devices either through waveguide and electrode design or active tuning of the multi–electrode biasing

structures. By extending a matrix representation of the coupled mode equations from a single coupling section to multiple coupling sections, the optical performance of a multi-section directional coupler will be optimized. Specifically, a single directional coupler has an optical transfer function:

$$\begin{pmatrix} As \\ Aa \end{pmatrix} = \begin{pmatrix} a112 & a122 \\ a212 & a222 \end{pmatrix} \begin{pmatrix} Aso \\ Aao \end{pmatrix}$$

Equation 1: Matrix representation of modal coupling between adjacent directional coupler waveguides

where the matrix elements are defined as:

$$a112 = (Cos[b2*L2]) + I*(((1/2)*dbeta*Sin[b2*L2])/b2)$$
$$a122 = ((I*X2*Sin[b2*L2])/b2)$$
$$a212 = ((-I*X2*Sin[b2*L2])/b2)$$
$$a222 = (Cos[b2*L2] - I*((1/2)*(dbeta/b2)*Sin[b2*L2]))$$

Equation 2: Coupled mode theory matrix coefficients

where dbeta represents the difference in propagation constants between the symmetric and asymmetric optical modes and L2 represents the length of the coupling section.

By extension, a multi-section directional coupler modulator is modeled as:

$$\begin{pmatrix} As \\ Aa \end{pmatrix} = \begin{pmatrix} a113 & a123 \\ a213 & a223 \end{pmatrix} \begin{pmatrix} a112 & a122 \\ a212 & a222 \end{pmatrix} \begin{pmatrix} a111 & a121 \\ a211 & a221 \end{pmatrix} \begin{pmatrix} Aso \\ Aao \end{pmatrix}$$

Equation 3: Three-electrode polymer modulator waveguide coupling in matrix format

A Mathematica™ simulation of the characteristic transfer function of a three-electrode directional coupler is shown below:
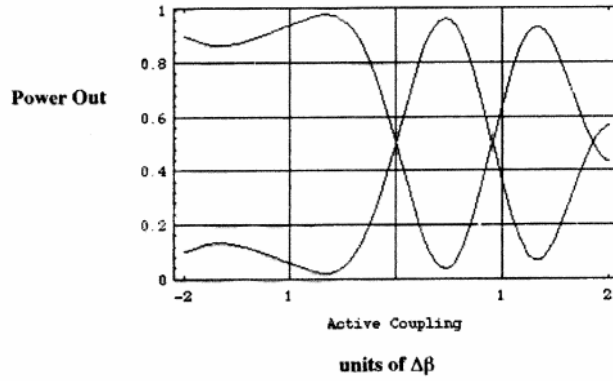
Figure 36: Mathematica™ simulation o f a three-electrode modulator E-O transfer function
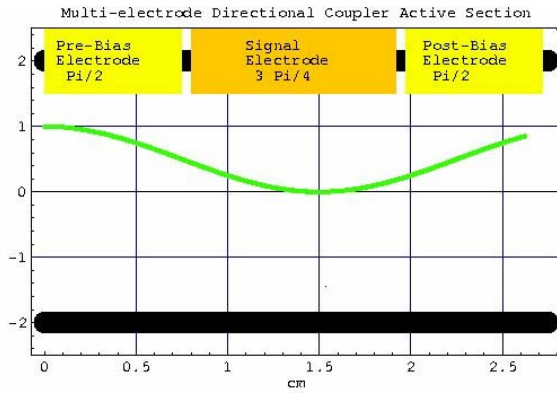
Figure 37: Multi-Electrode and waveguide layout
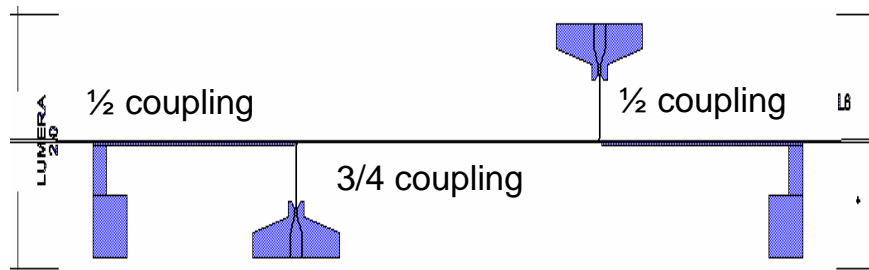
Figure 38: Mask layout of electrode including termination

26
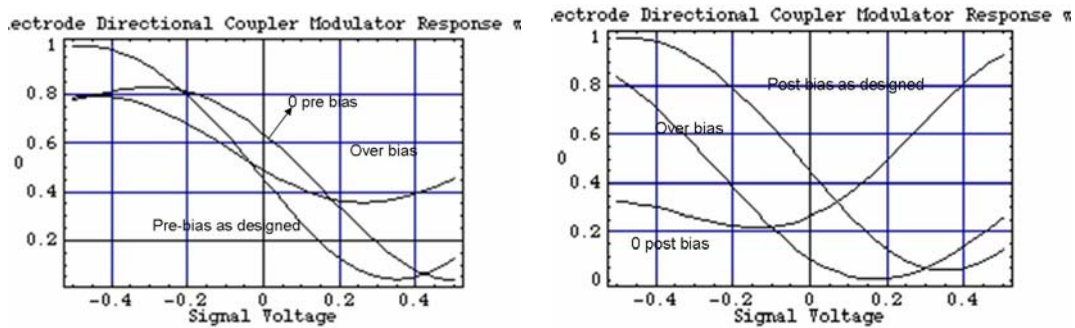
Figure 39: Mathematica™ prediction of bias voltage sensitivities. Left: pre-bias sensitivity, Right: post-bias sensitivity

Optimized three-electrode directional coupler simulations resulted in a simulated SFDR greater than 121 dB on a noise floor of 171 dB. These were calculated by running a Mathematica™ based numerical simulation on the analytical transfer calculated with the above described formulation.
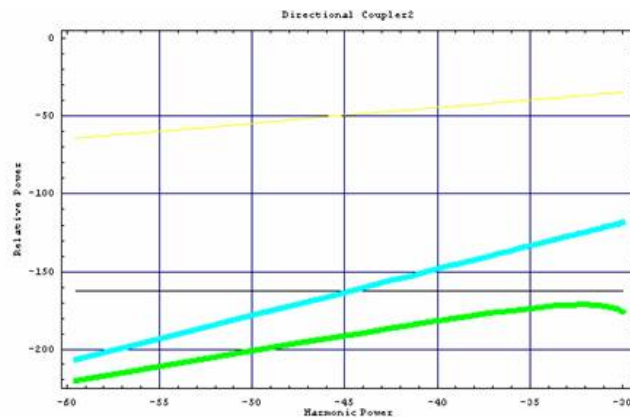
Figure 40: SFDR Calculation: Combined Mathematica™ program of a three-electrode SFDR response

Combining the optical design and simulations with Lumera polymer modulator techniques was accomplished and is described in the following polymer modulator wafer fabrication and optical testing results:

Lot X200-3: Active three-electrode directional coupler results:

Lot X200-3 contained active three-electrode directional couplers. The following results are a detailed optical test of a three-electrode directional coupler signal driven on the center drive only.
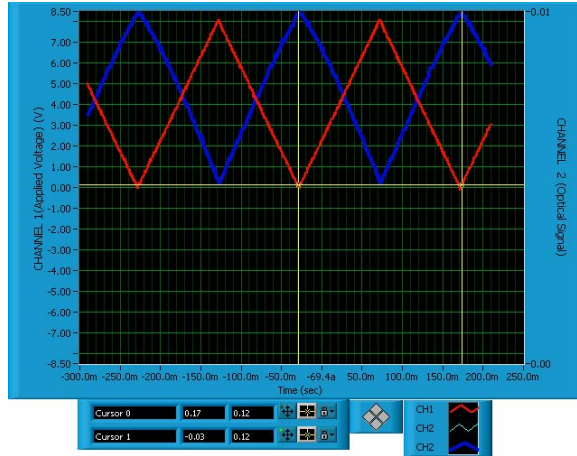
Figure 41: July 21 2004 Testing of Wafer 200-3 Air Force Cells:

Cell L-6 Build;UV-15 XL: 3 µm APC/DH6 27%:3 µm Quasi-Trench depth:.8 µm Un-Etched Core: 2.9 µm

Drive Section: 1.125 cm

Bias sections: .75 cm

Total active region: 2.625 cm

Test Condition for three electrode directional couplers:

No bias

+/- 4 V drive voltage, center electrode only, triangle wave 2 V bias
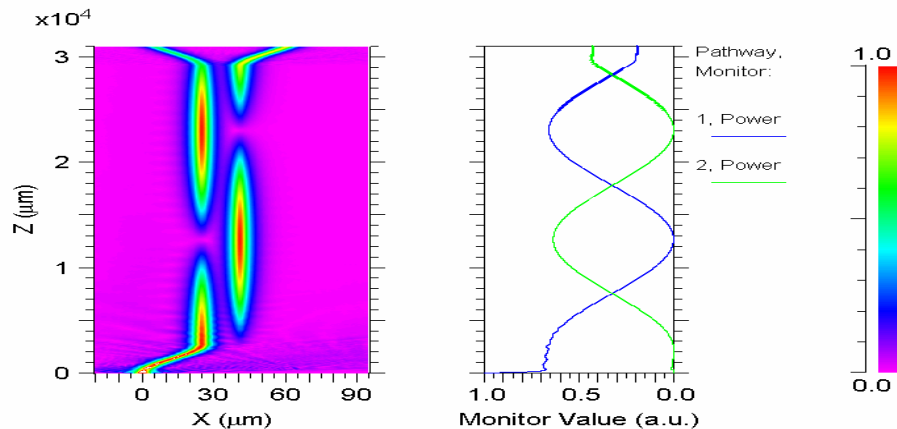
Figure 42: X200_3 Simulation of three-electrode directional coupler passive performance

Simulations of X200_3 and the measured optical response for zero bias condition modulator performance are presented. The device performance in the small signal region is shown on the LabView™ screen capture and the predicted optical path for the directional coupler waveguide

28

structure is also shown in the above graph. The three-electrode polymer modulators were fabricated on wafer X237-21 and X237-82. X237-82 was measured on the Lumera optical test station. SEM pictures (below) of X237-21 show a clearly defined quasi-trench optical waveguide with nominal width and size as modeled in the BeamProp™ simulations and the optical test results of a three-electrode directional coupler from lot X237-82:
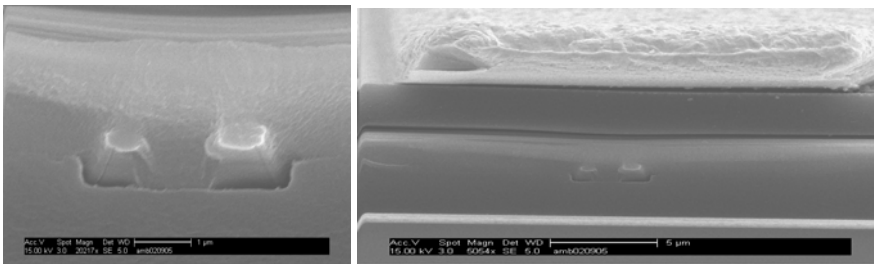
Figure 43: SEM Pictures of X237-21
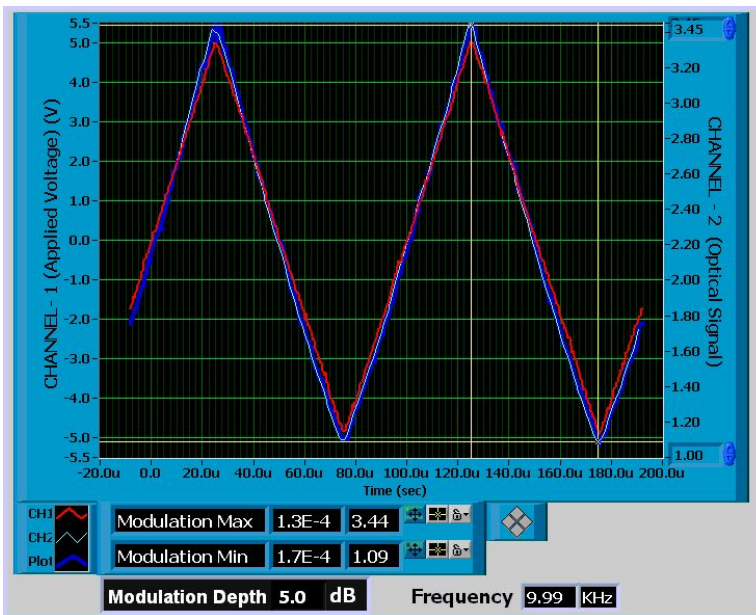
Figure 44: X237-82 three layer polymer stack with an RF signal microstrip electrode and pre- and post-bias electrode for electronic bias

29

2.2 New Advanced Modulator Designs: Splayed 3dB coupled Directional Coupler

A core focus of the advanced modulator modeling effort was transferring the technical concepts for splayed directional couplers to R-soft Beam propagation software, our masking and finite element beam propagation software. These splayed directional couplers are a second approach to achieving the requisite linearity in an optical modulator.

Splayed directional couplers have a nominal coupling gap which then increases as a function of the propagation direction, z, which effectively reduces the coupling efficiency between the waveguides. In order to model and optimize the effect of this distributed coupling, Prof. Mickelson generated mathematical constructs for defining the modal evolution of the optical fields in the region of the splayed directional coupler. The underlying representation within this analysis was a Stokes vector representation of the modes.

The parameters used were primarily the coupling strength between the two eigenmodes of the system as a function of the propagation direction, (Kappa), and the initial state of the optical eigenmodes, (both amplitude and phase). Since these are 3 dB coupled devices, (a splitter feeds both arms of the Mach-Zehnder optical fields of equal amplitude and zero relative phase between said optical fields) the initial amplitude of the antisymmetric mode is zero. By optimizing the SFDR the following modulation transfer function is obtained.

The coupling strength, Kappa, is the primary variable required to be mapped into the R-soft beam prop program. From the graph one can immediately note that the initial coupling strength is a factor of unity (the graph is normalized to Pi), and the final coupling strength was ~1/6. A coupling strength of one is such that the optical power is completely transferred from one guide to the other guide over that propagation distance, which for our devices is ~2.25 cm.
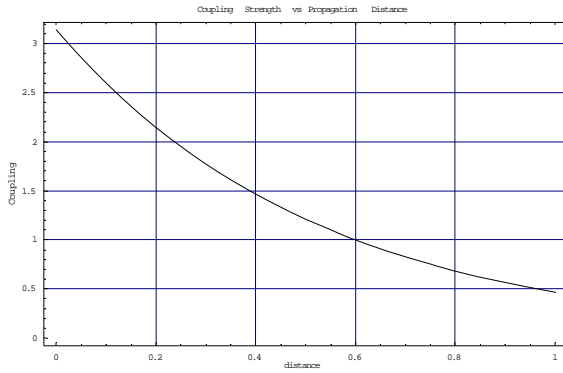
Figure 45: Coupling, (Kappa), between eigenmodes as a function of optical propagation (z)

Using these parameters the Spur Free Dynamic Range was calculated to be in excess of 118 dB using a noise floor of -160 dB (129 dB using a noise floor of -171 dB)
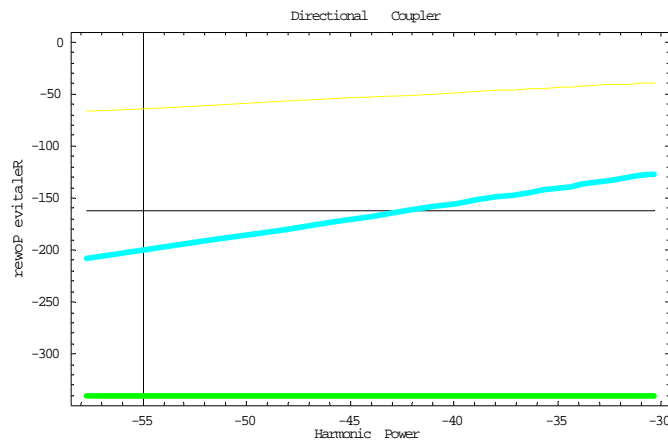
Figure 46: SFDR Calculation Splayed Directional Coupler

As a side note the shot noise floor used for the IEEE Photonics Technology Letters paper, V6 N2 of Feb 1994, Schaffner et.al., is -171 dB and the actual was -164 dB. Currently we are using -160 dB. So our noise floor calculations are somewhat conservative and using the -171 dB noise would give us an additional 9 dB of SFDR. This means the best devices, (both 3dB splayed couplers and three-electrode couplers), which show 115 dB would be 124 dB of dynamic range.

BeamProp™ is our current tool to generate the dxf files for prototype mask production. The following is a summary of the base calculations and sensitivities performed. A BeamProp™ physical device model mimicking those coupling parameters from Alan Mickelson's analytical

31

results for a splayed directional coupler was created and the following device performance curves were generated. The results were somewhat limited by computational noise and run times, (~200 hours for the following set of curves). Keeping the coupling length fixed, the finite element beam propagation software running as a scalar multi-layer simulation was run varying the initial gap, (the splay was set at 3.5 μm):
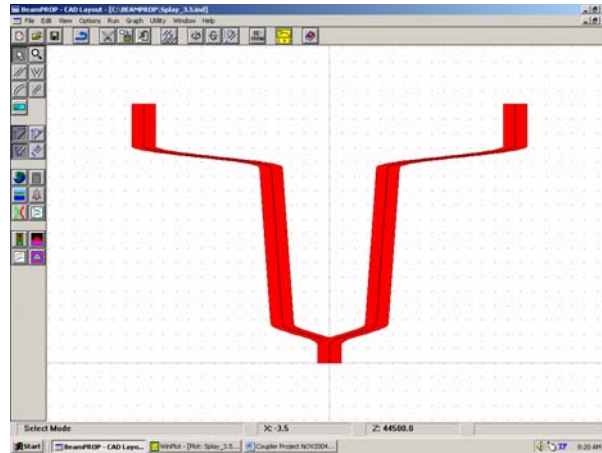
Figure 47: Splayed Directional Coupler
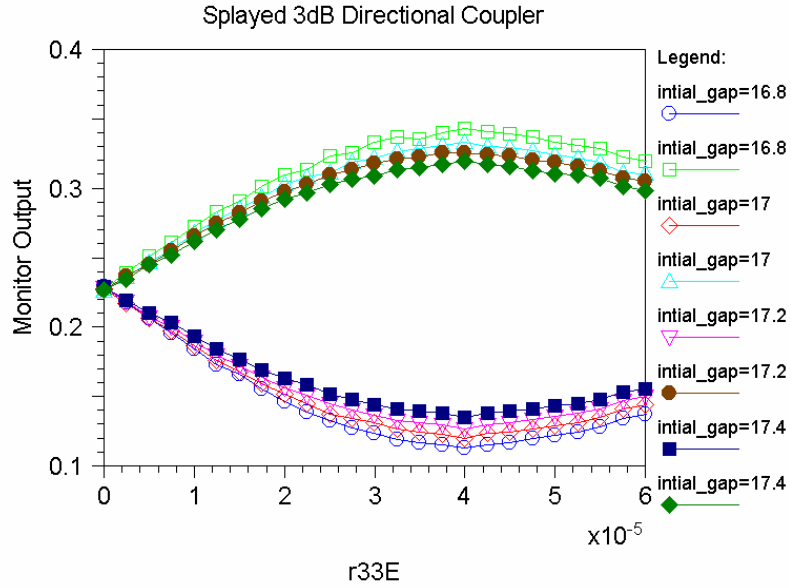
Figure 48: Splayed Directional Coupler Large Signal Regime (RSoFt Beam Prop™)

Note the modulation efficiency is ~1/2 that of an equivalent Mach-Zehnder modulator with a 14.2μm initial gap simulation with 3.5 μm of splay in the directional coupler:
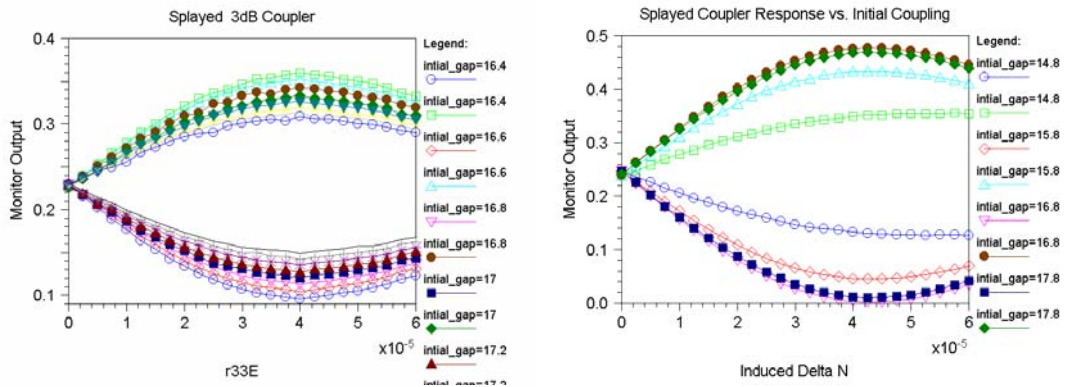
Figures 49, 50: Splayed Directional Coupler Large Signal Regime (RSoFt Beam Prop)

Translation of numerical results from BeamProp™ back into Mathematica™:

Beam Prop 3.5 um Splayed Directional Coupler
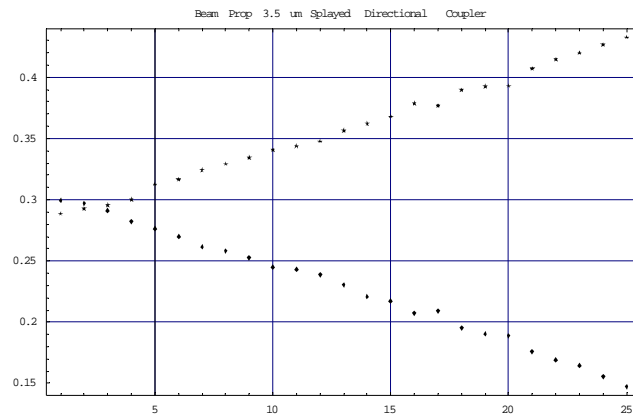
Figure 51: Splayed Directional Coupler Large Signal Regime (Mathematica™)

One can see computation noise in the BeamProp™ calculation is preventing deriving an accurate measure of the SFDR from these calculations. The general transfer function response was qualitatively very close to the analytical results. These new optical design concepts were incorporated into the Air Force hard mask set and the new mask generated was designated AirForceOne. Lot X260 was fabricated with this mask set and a designed experiment of chromophore concentration and cladding type was included in this final fabrication run.

2.2.1 Lot 260: Splayed Directional Couplers and optical loss of 22% DH6/APC vs 27% DH6/APC polymer core

The final process fabrication run was Lot 260. To our knowledge this was the first time a polymer 3 dB splayed directional coupler type modulator has been fabricated and tested. Presented below is the SEM of the polymer waveguide formed by the Lumera quasi-trench process and the poling profile utilized in the fabrication cycle for wafer 260-8.

- trench depth: 0.8μm
- core on top of trench: 2.05μm
- dip: 150μm
- waveguide width: 3.8μm
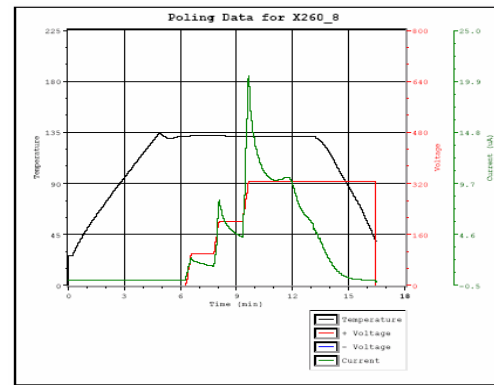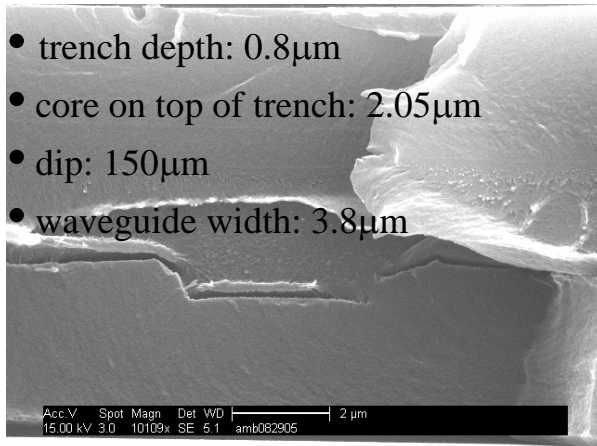
Figure 52, 53: X260-8 waveguide and poling profile

Straight waveguides were tested from the "'t" test cell, single mode waveguide operation was observed and the loss on the unpoled waveguides was measured with a single mode polarization maintaining fiber as the input and a large area New Focus detector on the out put. The insertion loss fiber to free-space was –9 dB. Standard Mach Zehnder modulators with a 2.5 cm active length were measured to quantify the poling efficiency and baseline the expected modulator performance
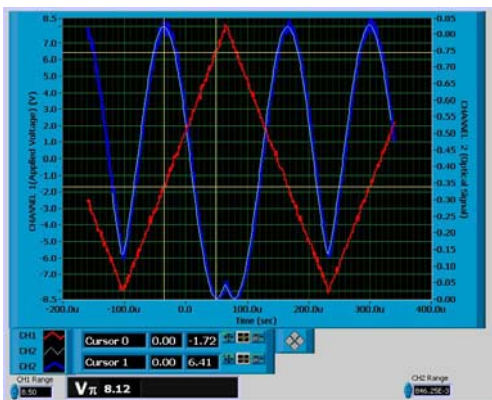
Vpi : 8.12 V modulation depth: 21 dB

Figure 54: Vpi was ~8 V for the 21% chromophore concentration under ~60 V μm poling conditions.

The 8.2 volts and 21 dB extinction ratio corresponds well with the 60 volts/ μm poling condition used to avoid poling induced loss. Splayed directional couplers were measured with a triangle wave electrical input and the following test data recorded:

Poling	Wafer-Poled
Mode Quality	Single-mode
Insertion Loss;	-14.5
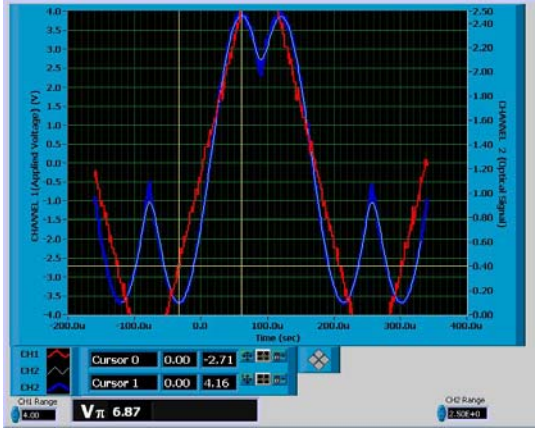
B3AbA3-Chip X260_5 0

Figure 55: Bias Free 3dB Splitter coupled Splayed Directional Coupler

Note that optical loss is measured on one output arm only of the Splayed directional coupler, for perfect splitting there will be 3dB differential when compared to Mach Zehnder insertion loss numbers. So 14.5 dB insertion loss for a 3 dB coupled directional coupler device is comparable   to -11.5 dB insertion loss on a Mach Zehnder modulator.

:
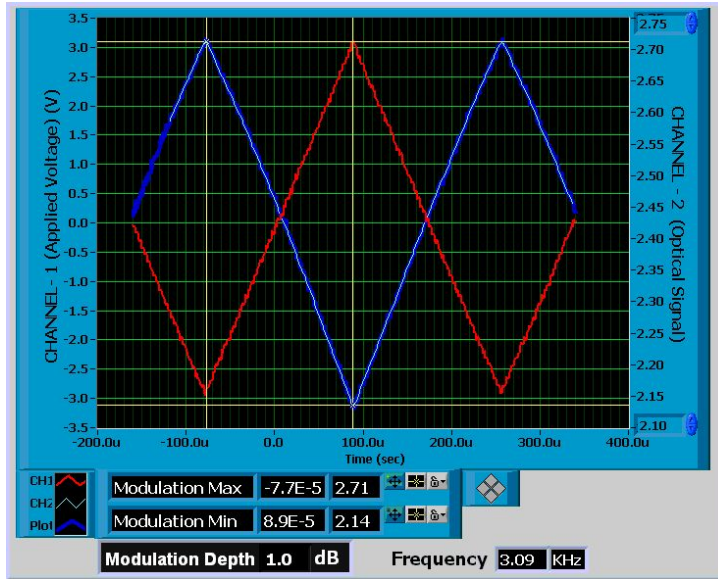
Figure 56: Small signal splayed directional coupler modulation results

Measurements of 3 dB coupled splayed directional couplers showed modulation characteristics that were qualitatively similar to those predicted in the BeamProp™ and Mathematica™ simulations. Because of two tone test limitations a quantitative test protocol of these devices was not performed; additionally the optical loss was calculated to be the main factor limiting SFDR. A strongly recommended future technical direction would be to lower the fiber coupled optical loss of these devices so that a true quantitative measure of the SFDR characteristics can be obtained with the U.C. Boulder SFDR optical test bed.

2.1.3. Design high frequency electrode structures for RF modulation of light

The following RF parameters were measured on Lumera fabricated microstrip polymer modulators with a polymer stack thickness of ~10 μm and nominal top electrode thickness of 21 μm. A Hewlett Packard network analyzer was used to measure the S21 and the smith chart of the frequency dependence of the input impedance:
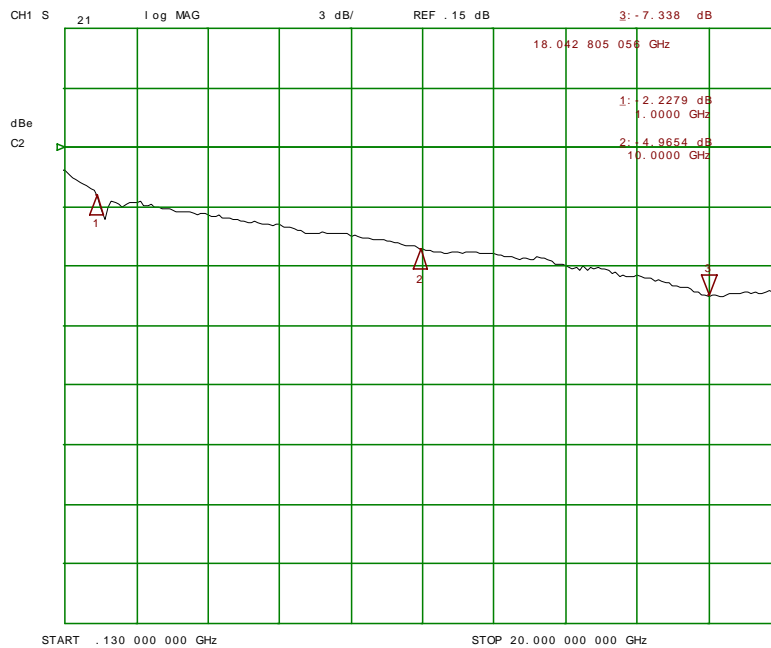
Figure 57: 260-2 A7 s21 Lumera 1 μm gold ground

Figure 58: X264-2 A8 Smith Chart:

Future transitions may be designed around smaller 50 μm spacing of the hot RF center electrode and the ground plane outer electrodes.

3.0 Conclusion and Future Technical Direction:

Highlights of the project are presented and future technical direction and current challenges are discussed. 3.1: Bias free modulators; 3.2: Electro-optic coefficient; and 3.3: Optical loss

Functional polymer modulators including multi-electrode and directional couplers were fabricated and tested. SFDR measurements were hindered by the poling induced and intrinsic loss of the guest host polymer systems being tested. Bias drift was variable throughout the program and 3 dB coupled devices were investigated as one way to overcome this limitation.

3.1 Bias Free Modulators

A 3 dB coupled directional coupler with an increasing separation between arms was modeled, fabricated and tested as a candidate for a bias free modulator.

Figure 59: Splayed 3 dB Directional Coupler

initial gap at the splitter = initial gap=12.5 µm
final gap at the far end = Splay= 8.28 µm

Future efforts may be directed at understanding the efficiency and SFDR characteristics of various initial and final waveguide separations. The possibility of a reversed electrode polarity on part of the coupled waveguide region needs to be investigated.
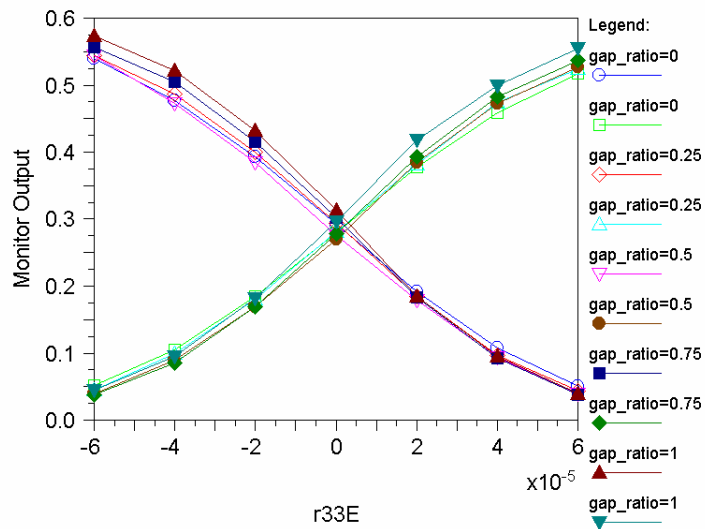
Figure 60: BeamProp™ of Splayed DC modulator small signal response for varying final to initial coupler gap ratios

Data from fabricated modulators indicates that the Lumera fabrication and polymer process is capable of producing polymer splayed directional couplers. Early results were qualitatively very promising and further study may show these designs can trade excess modulation depth for drive efficiency and still yield a SFDR greater than 124 dB.

3.2. Electro-optic coefficient

One of the key parameters of an optical modulator is the drive voltage, which is related to the half-wave voltage, V_π, which has a direct dependence on the r_{33}, the electro-optic coefficient of the material. Electro-optic organic polymers have demonstrated electro-optic coefficients around 100 pm/V @ 1310 nm [4] can be achieved by modifying the electronic properties of component chromophore to increase nonlinearity [5] while increasing the steric profile to overcome deleterious intermolecular dipolar interactions during poling.[4] Another important factor in device performance is loss of the electrical signal during encoding. There are three main factors that contribute to loss of the electrical signal in a functioning modulator at higher frequencies: 1) resistive loss in the electrode; 2) dielectric loss in the optical waveguide, which depends on loss tangent of the material; and 3) velocity mismatch between the electrical and optical signal. Electro-optic polymer devices promise both increased operating frequencies due to lower dielectric loss and lower dispersion as well as lower drive voltages due the increased r_{33}.

Lumera believes there are significant potential advantages to fabrication of multi-layer waveguide directional coupler modulators with our proprietary high performance electro-optic polymers in conjunction with NDC carbon nano-tube containing transition polymer layers between the bottom clad and the Au bottom electrode. It has been shown that in all-polymer electronic circuits the first few conductive polymer mono-layers next to the base polymer dominate the charge transport process[2]. It is also known that the energy barrier to charge injection from metallic

---

[2]   Spatially Correlated Charge Transport in Organic Thin Film Transistors
Biscarini **Phys. Rev. Lett.**. 92 116802 2004)

electrodes onto polymer chains takes place within 100 aryl units of the interfacial layer[3] making both the interfacial layer between the base polymer and the semi-conducting polymer and the morphology and chemical composition of the conducting polymer layer directly abutting the metal electrodes critical to polymer modulator electro-optic poling and in turn the modulation efficiency and bandwidth. It has been established that charge transport inside polymer systems is dominated by inter-chain hopping mechanisms. The following graph shows two orders of increase in the low frequency conductivity of polymer cladding material when used in conjunction with NDC electro-chemically generated 10 nanometer thick polymer transition layer between the bottom electrode and the bottom polymer cladding layer and a very desirable rolloff in conductivity at higher frequencies.
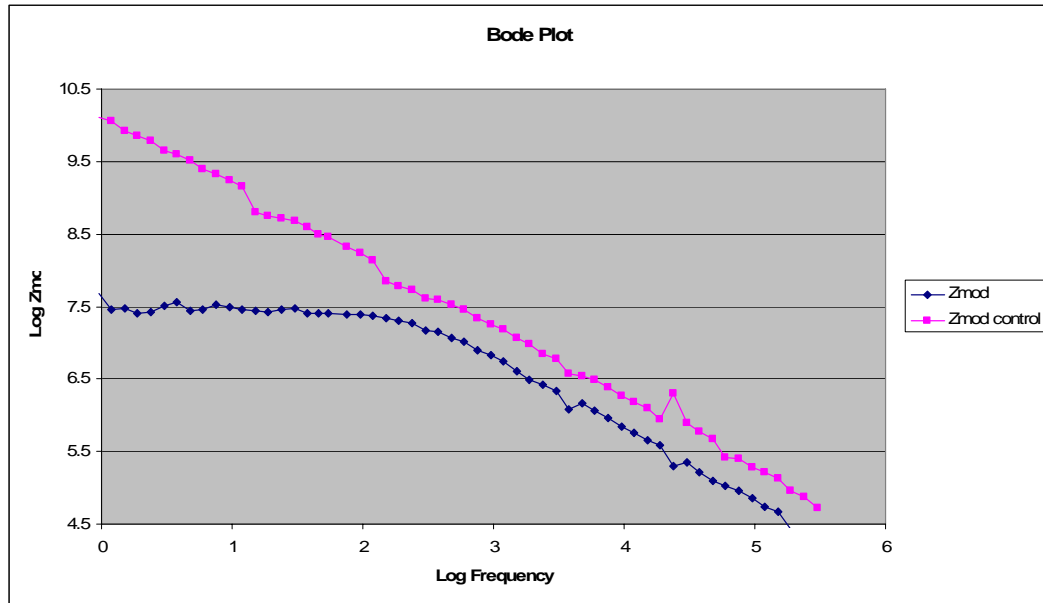
Figure 61: Complex Impedance Spectroscopy of polymer cladding impedance with (blue) and without (red) electrochemically deposited conductive polymer buffer layer between Au ground plane and polymer cladding material

Verification of the following predicted response / SFDR of biased polymer modulators is somewhat limited by the optical insertion loss of current generation polymer modulators and the DC drift; in part stemming from poling induced space charge fields generated in cladding layers during the

---

[3]   Understanding electron flow in conducting polymer films: injection, mobility, recombination and mesostructure **Journal of Physics: Condensed Matter 14** (2002) 9877-9898

poling process. To address the issue of space charge field at the boundary between the gold electrode and the polymer buffer, nanoMaterials Discovery Corporation (NDC) entered into a collaborative research and development program with Lumera to develop and to evaluate nanostructured materials used at the metal/cladding interface for improving DC conductivity properties of optical modulator devices. Under the aegis of this collaborative program, NDC developed a new conductivity screening methodology based on electrochemical impedance spectroscopy to allow evaluation of these materials using NDC's high throughput screening technologies. Subsequent high throughput screening identified a group of conducting polymer-carbon nano-tube nanostructured composite materials that show significant promise for improving DC conductivity through cladding materials. These improved DC conductivity levels were maintained through the thermal curing of the cladding material, which allows for improved process control during poling of the modulator devices. NDC demonstrated that its nanomaterials and manufacturing processes were versatile and could be used on both gold and indium tin oxide surfaces. Within the context of product development, NDC also addressed issues related to scaling the electrochemical manufacturing process for these new materials. As a result, NDC developed a manufacturing process that allows homogeneous electro-deposition of these nano-composite material films on large area electrode surfaces. The technology is well positioned at this time for incorporation into the product development process for optical modulator devices.

3.3 Optical Loss

The ability to tune the core clad index allows effective mode matching between the end face optical mode of the polymer waveguide and the small core fiber mode of the optical fiber used in pig-tailing the polymer modulators into packaged devices. Lumera's proprietary high-density plasma etching processes can generate polymer sidewall roughness as low as 50 nm (Figure 62a). Photolithography-dry etching feature control is depicted in Figure 62b.
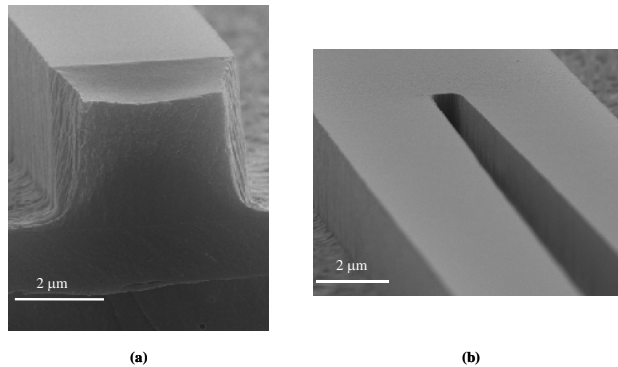
*Figure 62a: SEM micrograph of the waveguide side-wall
after high-density plasma etching; b: waveguide etched.*

Wall loss is critical to device loss and becomes a dominant device performance limiting process as the etch depth is increased in order to create the polymer wave guiding abilities for lower Δn polymer waveguide systems. Future polymer structures may incorporate lower Δn systems for better fiber coupling and this will help alleviate the optical loss problem for SFDR sensitive applications.

Fimmwave optical mode simulations show significant device improvement with the use of lower Δn (core/clad) polymer systems. The blue line in Figure 63 is a typically high Δn (core/clad) optical mode mismatch insertion loss (per face) and the orange line is a 1.60/1.585 Δn (core/clad) polymer waveguide. Approximately 2-3 dB of total device loss can be eliminated with the use of a lower Δn polymer waveguide.
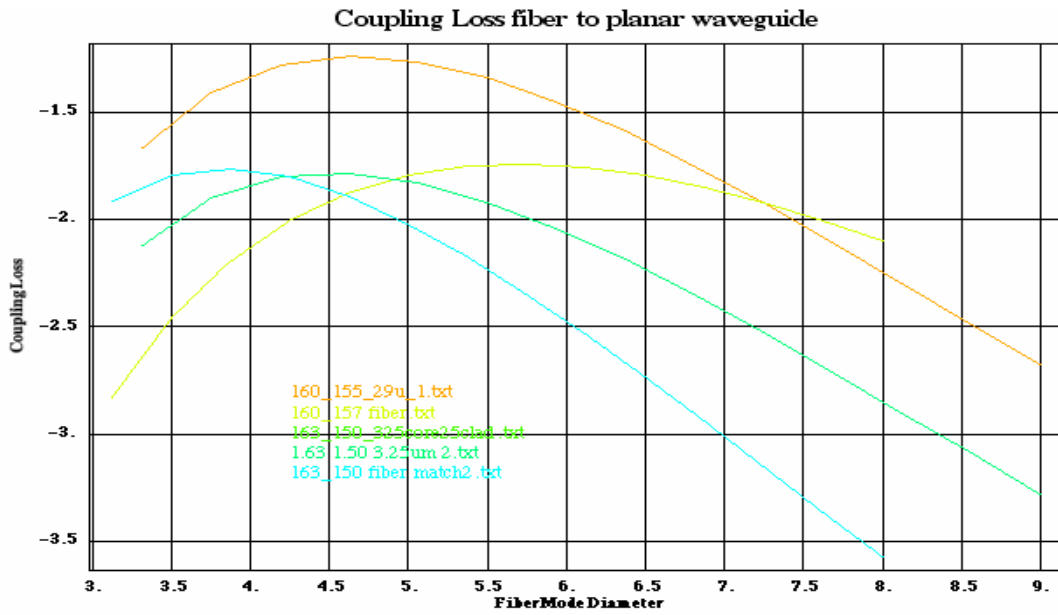
Figure 63: Fimmwave analysis of mode matching from three layer polymer waveguide to small core optical fiber

References:

[1] J.H. Schaffner, W.B. Bridges, *"Intermodulation Distortion in High Dynamic Range Microwave Fiber-Optic Links with Linearized Modulators"*, J. Lightwave Technol., **11**, 3-6, 1993.

[2] W.B. Bridges, J.H. Schaffner, *"Distortion in Linearized Electrooptic Modulators"*, IEEE Trans. Microwave Theory and Technol., **43**, 2184-2197, 1995.

[3] J.H. Schaffner, J.F. Lam, C.J. Gaeta, G. L. Tangonan, R.L. Joyce, M.L. Farwell, W.S.C. Chang, *"Spur-Free Dynamic Range Measurements of a Fiber Optic Link with Traveling Wave Linearized Directional Coupler Modulators"*, IEEE Photonics Technol. Lett., **6**, 273-275, 1994.

[4] Y. Shi, C. Zhang, H. Zhang, J. H. Bechtel, L. R. Dalton, B. H. Robinson, and W. H. Steier, "Low (sub-1-volt) halfwave voltage polymeric electro-optic modulator achieved by controlling chromophore shape," *Science*, **288**, 119-122, 2000.

[5] M. Lee, H. E. Katz, C. Erben, D. M. Gill, P. Gopalan, J. D. Heber, and D. J. McGee, "Broadband modulation of light by using an electro-optic polymer," *Science*, **298**, 1401-1403, 2002.

[6] S. Lin, W. Feng, J.C. Powelson, R. J. Feuerstein, L.J. Bintz, D. Tomic, A. R. Michelson, *"Scattering Induced Crosstalk in Active Directional Couplers"*, J. of. Lightwave Technol., **14**, 2021-2025, 1996.

[7] L. McCaughan, K.D. Choquette, *"Crosstalk in Ti:LiNbO₃ directional coupler switches caused by Ti concentration fluctuation"*, IEEE J. Quantum Electron., **QE-22**, 947-951, 1986.

[8] L. McCaughan, K.D. Choquette, *"Ti-concentration inhmogeneities in Ti:LiNbO₃ waveguides"*, IEEE J. Quantum Electron., **12**, 567-569, 1987.

[9] J. C. Powelson, W. Feng, S. Lin, R. J. Feuerstein, D. Tomic, *"Crosstalk of passive directional Couplers"*, J. of Lightwave Technol., **11**, 2020-2027, 1998.

[10] R. J. Feuerstein et al., "Equivalence of voltage bias and geometric waveguide design in directional couplers", *Appl. Phys. Lett.,* vol. 68, pp. 2775-2777, 1996.

Appendix A: System Analysis

Spur Free Dynamic Range

Mach--Zhender Modulators
Alan Mickelson
July 16, 2005
Edited by Lou Bintz
March 2006

Introduction

The spur free dynamic range (SFDR) is an important measure of the allowed range of operation of systems to be used for analog signal conversion from the electrical domain to the optical domain for transmission and then back to the electrical domain for further processing. Signal integrity within a given wavelength band requires that the second and higher order nonlinearities generate no beat notes that appear above the noise floor within the given wavelength band while the system is operating within the required range of signal amplitudes. An important system component in optical transmission systems for analog electrical signals is the optical modulator, that is, the component that converts the electrical signal to the optical domain by converting the electrical signal into optical intensity variations on an optical carrier. The Mach--Zhender interferometric modulator is a common type of modulator that can be used for this purpose. A schematic depiction of such a Mach--Zhender interferometric modulator is given in figure 1. The modulator is depicted as having a single optical input (on the leftright), a single optical output (on the rightleft) and a single microwave input (from above). The depiction ignores the optical reflection from the modulator which exits on the left, reflections from components to the right of the modulator that re--enter it from the right, microwave reflections that exit upward, and the microwave output (downward) that can also reflect energy back (upward) into the modulator. The modulator is actually an eight port device with four microwave and four optical ports. In what follows, we will see that detailed accounting for all of these reflections is unnecessary. The optical loss in propagating through the modulator is the single most important parameter for determining the SFDR. The electrical loss of the modulator actually does not show up in expressions for the SFDR, although it does affect the sensitivity of the system.
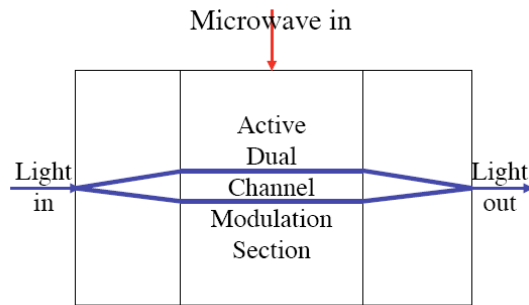
Fig1:A block diagram of a Mach--Zhender interferometric modulator that is assumed to modulate within some band of microwave frequencies. One should note that the microwave input generally needs to co--propagate with the optical wave in the active region and, therefore, a microwave termination is necessary. If one includes optical and microwave reflections back into the input ports and optical and microwave reflections from terminations back into the modulator, then the modulator becomes an eight (4 optical and 4 microwave) port device.

An Optical Transmission System for Electrical Signals

In this section we will discuss, piece by piece, an end to end system which takes an electrical signal, the output of a linear antenna, and transmits this electrical signal to a distant receiver on an optical carrier and converts the signal back to its ``original'' form in an optoelectronic converter. Attention is placed on the spectral characteristics of the system transfer function.

The transmission system

An optical transmission system may be seen to consist of an eight port modulator together with its inputs and terminations. Such a system is depicted in figure 1. The modulator is depicted here as having a single optical input from a continuous wave (CW) laser, (reflections back into the laser are ignored), a single optical output into a fiber link (reflections from further along the link are ignored), a single microoorwave input (reflections back to the antenna from the modulator are ignored) and the microwave line terminations
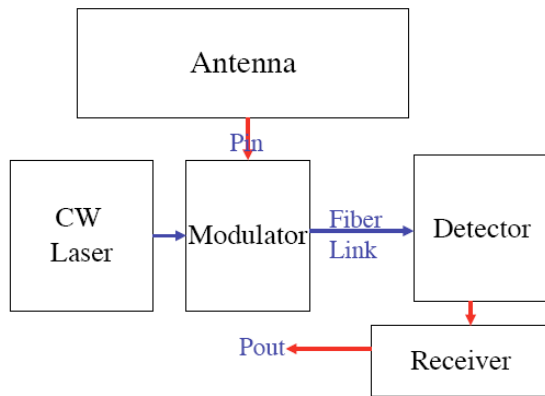
Fig 2 A rather typical block diagram of a microwave optical transmission system which includes an antenna signal as a microwave input, a continuous wave (CW) laser signal as an optical input, a modulator as a microwave optical transducer, a fiber link as a transmission medium, and then an optical detector and microwave receiver as a transduction subsystem back to the electrical (microwave) domain. Reflections from the modulator back into the laser, from the microwave feed point back into the antenna, from the (non--depicted) microwave termination back into the modulator and from the receiover back to the modulator have all been ignored foe simplicity of representation.

and line terminations and reflections from it are ignored. [4] The electrical input from above the modulator is the antenna signal and this signal is deposited in a termination that is a load impedance that we will call $Z_m = R_m + JX_m$ where the m stands for modulator, Z for impedance, R for resistance, X for reactance and j is the square root of minus one where complex monochromatic circuit signals are assumed to have a time variation of $\exp[j\omega t]$. The optical input to the left of the modulator box is a *pure* optical carrier, and the optical signal to the right is the optical signal with intensity modulation that is to be deposited in a square law optical detector. The square law optical detector is terminated by an impedance across which the output electrical signal is measured. Complex monochromatic optical signals are assumed to vary as $\exp[-i\omega t]$.

The electrical signal

The optical transmission system of the above example can be characterized by a transfer function. Before writing this function, though, we need to say something

---

[4]Sometimes an electrical output and optical input are ignored from each side in an *effective* four port representation. In this representation, electrical amplitude from above is converted to optical intensity on the right.

about the input electrical signal and then the assumed characteristics of the modulator in order to make the formulation tractable. Let us say that the electrical input signal was that taken directly off the terminals of the antenna. The signal can be characterized by an electrical power, P_{in}, that is the square of a zero mean signal on the antenna. The signal is zero mean as an antenna signal does not carry DC but instead can be represented as a sum of sinusoidal carriers which can be written in the normalized form

$$
\begin{aligned}
x(t) &= \Re\left[\sum_n |x_n| \exp[-i\omega_n t - i\phi_n]\right] \\
<x(t)>_t &= 0 \\
<\sqrt{x^2(t)}>_t &= \sum_n |x_n|^2 = 1
\end{aligned}
\tag{4}
$$

where $\Re$ denotes real, $|x_n|$ is the normalized amplitude of the sinusoidal signal component at angular frequency ω_n which has a phase shift ϕ_n relative to the other frequency components. The last equality is consequence of the normalization and the properties of sinusoids, where the angular brackets subscripted with the t denote a time average over a long enough (at least twice the longest beat note) period of the electrical carriers ω_n. FEvidently. for a signal to carry information, there must be a time varying modulation of the carriers. We will assume that the power level input to the antenna within the carrier band of interest varies much more slowly than the (microwave) carrier.

The optical modulator

The modulator is assumed to take an electrical input and convert it to an optical intensity modulation of the optical carrier, that is, the output of the CW laser that survives the modulator propagation path. In general, there will be an electrode loss L_e. As the loss incurs an exponential decay, it is a good approximation to say that the modulation voltage applied is that after the loss is incurred. (That is, an exponential function spends more time near its minimum than near its maximum). The input electrical voltage $V_{in}(t)$ and electrical input power P_{in} can be expressed as

$$
\begin{aligned}
V_{in}(t) &= \sqrt{P_{in} L_e R_m}\, x(t) \\
P_{in} L_e &= \frac{<\sqrt{V_{in}^2}>_t}{R_m}
\end{aligned}
\tag{5}
$$

where evidently the modulator impedance Z_m is assumed to be the real value R_m. The effect of the modulator is to take the input voltage and impress it on an optical carrier $\sqrt{P_{opt}}\exp[-i\omega_{opt}t]$ where P_{opt} is the optical power in the carrier. Generally, the modulator operation is defined by a transfer function $T(V_{in}(t))$ whose operation can be defined in terms of the optical power out of the modulator, $P_m(t)$, by

$$
P_m(t) = T(V_{in}(t))P_{opt}.
\tag{6}
$$

49

We have assumed that the function T is dimensionless. In order for this to be, it needs to be characterized by a parameter V_π where we will assume that when an input voltage of $V_{in}(t) = V_\pi \cos(\omega t + \phi)$ leads to a 50% power modulation index when ω falls within the system passband and that within the band, harmonic generation can be ignored. This is to say that under these restrictive assumptions, $2T(V_{in}(t)) \approx 1 + V_{in}(t)/V_\pi$. Because we will deal with nearly linear systems where the harmonic distortion is orders of magnitude below the fundamental, the above approximations are rather good.

The optical detection system

The detection system is the last of our considerations. TEvidently, the signal which exits the detector and is absorbed in the load shallould be called $P_{out}(t)$ and the load which absorbs it $R_L = Z_L - jX_L$ such that

$$P_{out} = \frac{\langle V_{out}^2(t) \rangle_t}{R_L} \tag{7}$$

where we will generally assume Z_L to be real for purposes of calculation, although this is not necessary. The signal entering the detector must include all the system losses between modulator and detector surface, losses that we will refer to as L_{opt}, so that the power incident of the detector should be $L_{opt} P_m(t)$. As the detector is assumed to be a perfect square law detector, the operation of the detector is take an input power and convert it to a current $I_{out}(t) = V_{out}(t)/R_L$ by the rule

$$I_{out}(t) = R_{sp} L_{opt} P_m(t) \tag{8}$$

where R_{sp} is the detector responsivity. The *square law* power out is then

$$P_{out} = R_{sp}^2 L_{opt}^2 \langle P_m^2(t) \rangle_t R_L \tag{9}$$

where evidently the time average in the last equation is going to be over the incident signal $x(t)$. This is the form of the signal that we need to perform loss budgeting of the system. Substituting for $P_m(t)$ from equation (6), we find

$$P_{out} = R_{sp}^2 L_{opt}^2 P_{opt}^2 R_L \langle [T(V_{in}(t))]^2 \rangle_t . \tag{10}$$

Table 1 gives a large array of possible values. The last column of that table gives values that were used in a 1995 paper by Bridges and Shaffner [1]. Using these values, we see that when P_{opt} is 100 mW and the optical path losses are 10 dB, the conversion factor of R_{sp} will give a current of 7mA. This then would correspond to a DC receiver power of 2.5 mW. Only a fraction of this is actually microwave modulated, though. When the V_π is 10 V, then full modulation requires a microwave power of 1 W when there is no microwave electrode loss. At full modulation, 1.25 mW of microwave power would appear at the output as only 50% of the light can carry microwave signal in intensity modulation. A modulation of V_π would clearly be strongly in the nonlinear regime. Every extra dB of optical path loss above the 10dB will lower the microwave output power by 2 dB. Every dB osf electrode loss will lower the output power by 1 dB.

This electrode loss, however, will also lower the effective voltage to a value less than V_π, so that the nonlinearity of operation is reduced. When the optical insertion loss is 30 dB and the microwave electrode loss in 20 db, then the received microwave power is reduced by 60 dB to roughly 1 nW. With 40 dB of total optical path loss and 30 dB of electrode loss, a V_π modulation results in 1 pW of microwave power. There is little or no dynamic range of the system left when there is only 1 pW in the reciver. That is, 1 pW cannot significantly exceed the noise floor of the system. Such consideration leads to the necessity for an SFDR definition.

The time averaged form of the signal is not really the one we want in order to define SFDR. We need to know something more about information content in order to discuss information transmission. Generally, the detector will output into an electrically band limited system and what we are interested in is the power spectrum of the signal within the band of interest. This is our next topic.

The system transfer function

A transfer function is generally a frequency domain quantity. Defining the Fourier transform pair by

$$
\begin{aligned}
f(\omega) &= \int_{-\infty}^{\infty} dt' f(t') \exp[i\omega t] \\
f(t) &= \frac{1}{2\pi} \int_{-\infty}^{\infty} d\omega f(\omega) \exp[-i\omega t].
\end{aligned}
\tag{11}
$$

We are dealing with actual signals, though. We do not want terms in our expressions which grow linearly with the time of signal integration. It is more realistic then to deal with time averaged spectra which take the form

$$
\begin{aligned}
f(\omega) &= < \frac{1}{\tau} \int_{t-\tau}^{t} dt' f(t') \exp[i\omega t] >_t \\
&= \frac{1}{N} \sum_{i=1}^{N} \int_{t_i-\tau}^{t_i} dt' f(t') \exp[i\omega t]
\end{aligned}
\tag{12}
$$

where the $f(\omega)$ has the dimensions of a Fourier component rather than a Fourier transform. The operations of the above equation mimic those of a spectrum analyzer rather closely. Ideally, we would like to obtain a transfer function relation of the form $P_{out}(\omega) = T_{sys} P_{in}(\omega)$ where the output and input power spectral densities can be expressed as

$$
\begin{aligned}
P_{out}(\omega) &= I_{out}^2(\omega) R_L \\
P_{in}(\omega) &= \frac{V_{in}^2(\omega)}{R_m}
\end{aligned}
\tag{13}
$$

when the (time averaged) current and voltage spectra are suitably defined, such as by a time average transform. The spectrum of the output current and the input output power relation are expressible as

$$
\begin{aligned}
I_{out}(\omega) &= R_{sp} L_{tot} P_{opt} \big[T(V_{in}) \big](\omega) \\
P_{out}(\omega) &= R_{sp}^2 L_{tot}^2 P_{opt}^2 R_L \, | \big[T(V_{in}) \big](\omega) |^2
\end{aligned}
\tag{14}
$$

where $L_{tot} = L_{mod} L_{opt}$ is the total loss in the optical path andwhere L_{mod} is the loss from the source output to the modulator output. The output current relation is not of the form $I_{out}(\omega) = TV_{in}(\omega)$ which would be required for $P_{out}(\omega)$ to be linearly related to the input spectra. Instead the T operates on the V_{in} before the average before the time average transform is taken. Any deviation of the T from perfectly linear response then will show up as nonlinearity and give rise to the harmonics that limit the SFDR. It is the unavoidable[5] curvature of the modulation transfer that gives rise to the higher harmonics. We will soon see that it is hard to change the T function appreciably enough to have much effect on the magnitude of the SFDR. We will see that there are a number of other controlling parameters that do have appreciable effect on the magnitude of the SFDR.

To say something about the system from either theoretical plots of the system behavior from system measurements, we need some additional simplification . This is best done in two steps. First, we expand the modulator transfer function as a power series such that

$$T(\sqrt{P_{in}L_eR_m}\,x(t)) = \sum_n T_n \left[P_{in}L_eR_m\right]^{\frac{n}{2}} x^n(t) \tag{15}$$

where for an ideal linear modulator would have $T_0 = 0.5$, $T_1 = \dfrac{1}{2V_\pi}$ and all other T_n

equal to zero. A Mach--Zhender interferometric modulator could exhibit such a transfer function for small signals if either stringent fabrication tolerances are met or if an electrical bias is applied to the electrodes. Such a modulator would not necessarily be lossless as we have taken loss into account with the optical loss term L_{mod} and the electrical loss term L_e. We next simplify the forms for our inputs. In general, there are two input forms that are used for spur free dynamic range (SFDR), one for theory and one for measurement. These forms are

$$\begin{aligned} x(t)|_{theory} &= \sqrt{2}\cos(\omega t) \\ x(t)|_{measure} &= \sqrt{2}\left[a_1\cos(\omega t) + \sqrt{1-a_1^2}\cos((\omega+\Delta\omega)t)\right] \end{aligned} \tag{16}$$

where we have assumed that $a_1 \leq 1$. The $\sqrt{2}$ in the above is to preserve the time averaged power normalization.

Defining SFDR

In order to define the SFDR, we generally use a single sinusoid at a frequency ω. When we do, the output power spectral density will have components at all integer multiples of ω. We could write that

$$P_n = P_{out}(n\omega)$$

$$= R_{sp}^2 L_{tot}^2 P_{opt}^2 R_L F_n \left[\frac{P_{in} L_e R_m}{V_\pi} \right]^n \tag{17}$$

$$= R_{sp}^2 L_{tot}^2 P_{opt}^2 R_L C_n P_{in}^n$$

where the last equality serves to define the nth order factor P_n, the F_n are algebraic factors which come from re--collecting terms of the Fourier expansions after multiplication by the T_n expansion coefficients. These F_n terms are the ones that express the linearity of the modulator response. These coefficients are all of order 1 in the sense that if we consider that $P_{in} L_e R_m$ is always less than V_π for purposes of our calculation here, the dominant behavior each order in the expansion is given by the term raised to the power n.

For our ideal linear modulator,

$$P_0 \approx \frac{R_{sp}^2 L_{tot}^2 P_{opt}^2 R_L}{2}$$

$$P_1 \approx \frac{R_{sp}^2 L_{tot}^2 P_{opt}^2 R_L}{2} \frac{L_e R_m}{V_\pi} P_{in}$$

$$P_2 \approx 0 \tag{18}$$

$$P_3 \approx \frac{R_{sp}^2 L_{tot}^2 P_{opt}^2 R_L}{2} F_3 \left[\frac{L_e R_m}{V_\pi} \right]^3 P_{in}^3$$

where the last two equations are consequences of the first two, at least in the case of the balanced Mach--Zhenders. That is, when the Mach--Zhender is *balanced* such thate P_0 and P_1 are as we have written, the phase between the arms is controlled, either through fabrication or by a bias voltage, such that there is no response at the second harmonic. This can be hard to acheieve in a Mach--Zhender configuration where an extra phase shift of $\pi/2$ radians is necessary before the arms are recombined. Y--junction inputs to directional couplers are automatically balanced without excess phase shift when they are not recombined.

Quite generally, the P_0 will be out of band. It may be the factor that determines the noise floor, however, if the P_0 is sufficiently large that the receiver noise is shot noise limited. The receiver noise may be dominated either by shot noise, thermal noise or the relative intensity noise (RIN) of the laser. The thermal noise power in the receiver in a one Hertz bandwidth is given by Boltzmann's constant k times the temperature T. At room temperature, this factor is roughly 0.026 eV which corresponds to a noise power of -172 dBm. The shot noise power of a 10 mW optical input leads to a shot noise power of roughly -164 dBm. The laser RIN can be greater or smaller than this number.

The SFDR is defined as the ratio of the power in the first harmonic to the noise floor at the input power at which the third harmonic crosses the noise floor. Denoting the noise floor as N_f, we can write that

$$SFDR = P_1(P_3(P_{in}) = N_f)/N_f. \tag{19}$$

Using the above relations, we see that $P_3 = N_f$ when

$$P_{in}(P_3 = N_f) = N_f^{\frac{1}{3}} \left[\frac{V_\pi}{L_e R_m} \right] \left[\frac{2}{R_{sp}^2 L_{tot}^2 P_{opt}^2 R_L} \right]^{\frac{1}{3}} \left[\frac{1}{F_3} \right]^{\frac{1}{3}} \tag{20}$$

which gives that

$$P_1(P_3(P_{in} = N_f) = N_f^{\frac{1}{3}} \left[\frac{R_{sp}^2 L_{tot}^2 P_{opt}^2 R_L}{2} \right]^{\frac{2}{3}} \left[\frac{1}{F_3} \right]^{\frac{1}{3}}. \tag{21}$$

Interestingly, the electrical characteristics V_π, L_e and the modulator matching resistance R_M have fallen out of the expression. The SFDR is not dependent on these quantities. If the drive requirement goes up, all curves scale up accordingly. The sensitivity of the system is reduced, but the SFDR does not give any information about sensitivity. Normalizing to the noise floor, we find

$$SFDR = \left[\frac{1}{N_f} \right]^{\frac{2}{3}} \left[\frac{R_{sp}^2 L_{in}^2 P_{opt}^2 R_L}{2} \right]^{\frac{2}{3}} \left[\frac{1}{F_3} \right]^{\frac{1}{3}}. \tag{22}$$

An interesting point here is the extremely weak sensitivity of the form of the transfer function T. It can be hard to change the harmonic of the function appreciably, yet even if we do, the one third power is a real damper. A change of harmonic content of the T will only change the SFDR by roughly a factor of two. With the electrical drive path falling out of the equation and the modulator transfer function being only peripherally important, we see that optical loss is the factor which determines the SFDR. Yet there is a limit on the optical power we can pump in. It is the modulator loss and how closely the channels can be made to be match those of the transmission medium (minimization of coupling loss) that determine the SFDR. All other effects are higher order.

If we use the Bridges Shaffner values of from the last column of table 1, we find that the SFDR is roughly 110 dB as is illustrated in figure 3. The Bridges Shaffner values assume that the noise floor is

130mmSFDR

A plot of the noise floor, the first order signal, third order distortion signal and a line indicating the value of the input power at which the third order intercept crosses the noise floor. It is the difference between the output power at the third order intercept (with the noise floor) and the first order signal value at that ordinate that is the spur free dynamic range (SFDR). This plot is made for a purely sine wave transfer function (ideal, perfectly biased Mach-Zhender) with the Bridges Shaffner parameters. The SFDR for these parameter values is about 110 dB.

Factor Minimum Maximum Bridges--Shaffner

N_f $2kT \approx -172$dBm $RIN \approx -100$dBm $(2e)(R_{sp})(2.5\text{mW})(50\,\Omega) \approx -160$dBm

V_π 0.5V 20V 10V

54

$$L_e \quad \text{0dB 20dB 0dB}$$

$$R_m \quad 10\Omega \ 1\text{k}\Omega \ 50\Omega$$

$$R_{sp} \quad 0.1\text{A/W} \ 1.5\text{A/W}(0.85\mu\text{m}) \ 0.7\text{A/W}$$

$$L_{tot} \quad \text{0dB 50dB 10dB}$$

$$P_{tot} \quad 100\,\mu\text{W 1W 100mW}$$

$$R_L \quad 10\Omega \ 1\text{k}\Omega \ 50\Omega$$

$$F_3 \quad 0.01 \ 0.5 \ \text{variable with nominal M--Z value 1/6}$$

The system parameter values in the order that they appear in the equation for P_{in} at the third order noise floor intercept. The values originally used by Bridges and Shaffner in a 1995 paper are included in the last column and also are used in the *SFDR* plot included for scaling purposes. determined by the shot noise of the laser source. We also could be in limits where the noise floor is thermal noise limited or the limit where the noise floor is determined by the laser RIN. Generally, the shot noise limit is that with the greatest SFDR and the RIN limited one the worst of the three. Let's now consider these three limits individually.

Shot Noise Limit

In the shot noise limit, the shot noise power (per Hz)

$$P_{sn} = 2eR_{sp}L_{tot}P_{opt}R_L \tag{23}$$

where e is the electron charge $e \approx 1.610^{-19}$ coul, must exceed the thermal noise power (per Hz)

$$P_{tn} = 2kT \tag{24}$$

as well as the laser *RIN*. Practically, the received optical power here must be on the order of hundreds of μ Watts and the laser *RIN* less than roughly -172 dBm per Hz. These values are achievable for very quiet sources and low ($\leq \approx 15$dB) total (all couplers as well as modulator insertion) optical loss. In this limit, we can replace the P_{nf} in 22 with the equation (23) for P_{sn} to obtain

$$SFDR(P_{sn}) = \left[\frac{R_{sp}L_{tot}P_{opt}R_L}{4e}\right]^{\frac{2}{3}}\left[\frac{1}{F_3}\right]^{\frac{1}{3}}. \tag{25}$$

The SFDR increases more slowly with optical source power in this limit. The input facet of the modulator will certainly exhibit a power density limit so the only way to maximize the SFDR for a high power low RIN laser is to minimize the optical path loss.

Thermal Noise Limit

When the laser *RIN* is less than about -172 dBm (per Hz), then even with significant path loss, it is possible to reach the thermal noise limit characterized by

$$SFDR(P_{tn}) = \left[\frac{1}{2kT}\right]^{\frac{2}{3}}\left[\frac{R_{sp}^2 L_{tot}^2 P_{opt}^2 R_L^2}{2}\right]^{\frac{2}{3}}\left[\frac{1}{F_3}\right]^{\frac{1}{3}}. \tag{26}$$

The SFDR here increases the received power raised to the 4/3, double the slope on the $\log$ -- $\log$ plot of the SFDR in the shot noise limit.

Laser RIN Limit

When the laser RIN exceeds the thermal noise, the expression is similar to 26 except that the laser RIN (per Hz) replaces the $2kT$, such that

$$SFDR(P_{tn}) = \left[\frac{1}{RIN}\right]^{\frac{2}{3}}\left[\frac{R_{sp}^2 L_{tot}^2 P_{opt}^2 R_L^2}{2}\right]^{\frac{2}{3}}\left[\frac{1}{F_3}\right]^{\frac{1}{3}}. \tag{27}$$

This is the limit obtained when the source is not designed for low noise, and the path loss is equal to or greater than commercial values for $LiNbO_3$ modulators, for example, where the specification on total fiber to fiber optical insertion loss is less than 10 dB leading to a link budget of minimally 15dB when other connectors are included. The Bridges--Shaffner [1] number for noise floor is -160 dBm (per Hz) so that a modulator with -140 dBm (per Hz) will start with a 13.5 dB SFDR penalty relative the a Bridges--Shaffner system. An optical path loss of 30 dB in this RIN limit will then penalize one by another 26.5 dB relative to Bridges--Shaffner. As a good Mach--Zhender will give about 110dB SFDR A system with 30 dB path loss and 140 dB RIN will have a total Bridges--Shaffner penalty of roughly 40 dB, and will then come in with an SFDR of roughly 70 dB.

References

[1] W. B. Bridges and J. H. Shaffner, Distortion in linearized modulators, IEEE transactions on Microwave Theory and Technique 43, 2184-2197 (1995).

[2] R. J. Feuerstein, W. Feng, J. C. Powelson, S. Lin, L. Bintz and A. R. Mickelson, Equivalence of voltage bias and geometric waveguide design in directional couplers, Appl. Phys. Lett. 68 (20), 2775-2777 (1996).

[3] J. H. Shaffner, J. F. Lam, C. J. Gaeta, G. L. Tangonan, R. L. Joyce, M. L. Farwell, and W. S. C. Chang, Spur--free dynamic range measurements of a fiber optic link with traveling wave linearized directional coupler modulators, IEEE Photonics Technology Letters 6, 2, 273--275 (February, 1994).

[4] T. R. Halemane and S. K. Korotky, Distortion characteristics of optical directional coupler modulators, IEEE tranactions on Microwave Theory and Technique 38, 5, 669--673 (1990).

[5] G. E. Betts, Linearized modulator for suboctave--bandpass optical analog links, IEEE transactions on Microwave Theory and Technique 42, 12, 2642--2649 (December 1994).

[6] G. J. Foschini and C. D. Poole, Statistical theory of the polarization dispersion in single mode fibers, Journal of Lightwave Technology 9, 1439-1456 (1991).

[7] C. D. Poole, J. H. Winters, and J. A. Nagel, Dynamical equations for the polarization dispersion, Opticsl Letters 16, 372-374 (1991).

Appendix B: Initial data and Results on the UC Boulder SFDR Test Bed

1. Electro-optical modulator characterization

The goal of the project is to determine the spur free dynamic range (SFDR) of Lumera's electro-optic modulators. During the course of the evaluation, it was determined that the optical and microwave losses of the modulators were too large to get an SFDR measurement. The following report contains a summary of modulator characteristics and the measurement techniques used to determine them

2 Equipment

IPG Photonics Erbium Fiber Laser ELD-1 HP 70950A Optical Spectrum Analyzer HP 8671B Synthesized CW Generator (2-18 GHz) HP 8349B Microwave Amplifier (2-20 GHz) HP 437B Microwave Power Meter HP 6624A System DC Power Supply Picosecond Pulse Labs Bias-Tee 5550B HP 8562A Spectrum Analyzer Keithley 199 DMM/Scanner ThorLabs B5015 Beam Splitter Discovery Semiconductor DSCR401ER High-speed Detector Newport 818-IR Detector ThorLabs 2x2 fiber coupler 10202A-50-FC Cascade Microtech Probe ACP40-AW G5G-450 Cascade Microtech Probe Arm 101-118 x20, 0.40 NA Microscope Objective Panasonic Monitor 990
3 Experimental Setup and Data

3.1 Erbium fiber laser (EFL) spectrum

The EFL spectrum is measured using an HP 70950A optical spectrum analyzer (OSA). The spectrum is illustrated in Figure 1.
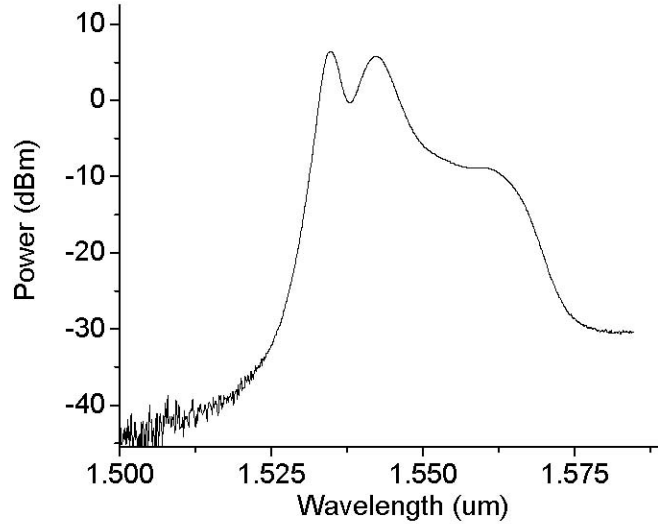
Figure 1: The spectrum of the IPG Photonics erbium fiber laser (EFL) source. The RIN of the source was measured to be approximately -140 dB/Hz.

3.2 EFL relative intensity noise (RIN)

The setup to measure the erbium fiber laser (EFL) relative intensity noise is illustrated in Figure 2. In the setup the spectrum analyzer is set to determine the noise in 1 Hz bandwidth at 8 GHz (SFDR measurement frequency). The optical power meter is then used to determine the average optical power in the signal. The measured RIN will also contain contributions from the shot noise and thermal noise fluctuations. The RIN of the laser can be extracted from the measured RIN using the following relation:

$$RIN = \left(\frac{\Delta P}{P_{avg}} \right)^2$$

$$RIN_{laser} = RIN_{measured} - \frac{2q}{I_{dc}} - \frac{P_{thermal}}{P_{electrical}}$$

where *Idc* is the electrical current, *Pthermal* is the thermal noise current and *Pelectrical* is the average electrical power.
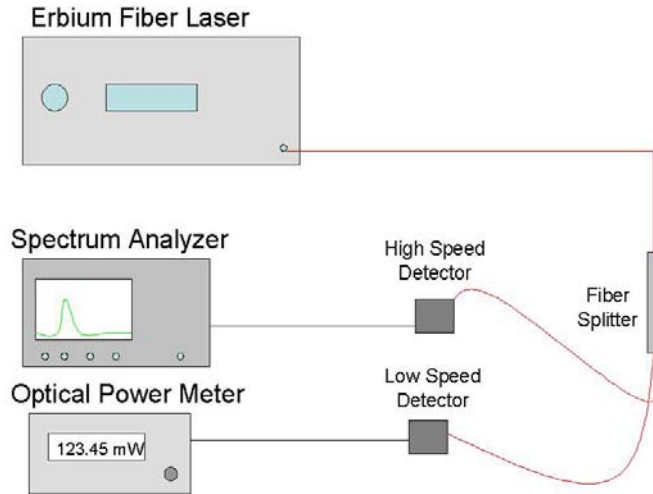
Figure 2: Picture of the setup used to measure the RIN of the laser source.

3.3 Microwave characteristics (2-12 GHz)

The microwave source output power was calibrated using the HP 437B microwave power meter. After the calibration the loss in the cables was measured from 2-12 GHz. The Cascade Microtech probes and the modulators were then inserted into the system and the microwave insertion loss was measured from 2-12 GHz. The measurement results are illustrated in Figure 3. It is clear that the insertion loss of the modulator and probes is quite large.
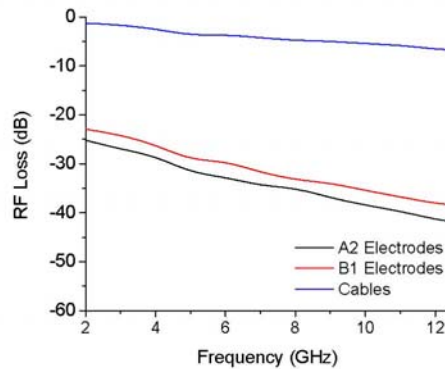

Figure 3: Loss for cables and the electrodes of modulators A2, B1

3.4 Modulator electro-optic characteristics

The setup used to determine the electro-optic characteristics of the modulators is illustrated in Figure 4.

60
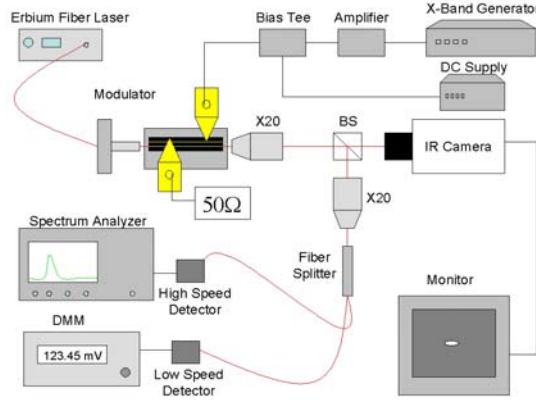
Figure 4: Picture of the setup used to measure the modulator parameters.

Vπ for the devices was determined using a low frequency sinusoidal signal. The result is illustrated in Figure 7.

The modulator frequency response, T(f), was determined by holding the input RF power and input optical power constant and varying the frequency of the RF input signal. The DC bias at the input of the modulator is set to $V\pi/2$. The results are illustrated in Figure 8.

The amplitude transfer function, T(V), for the modulator is determined by holding the amplitude of the optical input constant and varying the amplitude of the RF signal. A majority of the loss is clearly due to the modulator. A frequency sweep of the probes on a through test substrate provided by Cascade Microtech is illustrated in Figure 5.
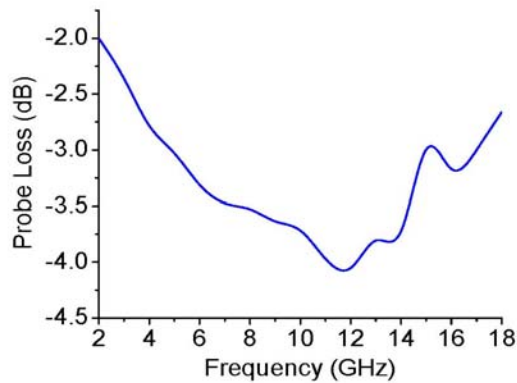

Figure 5: Cascade probe losses on a 50 Ohm through test substrate.

Modulator measurement results are illustrated in Figure 6 and Figure 7.
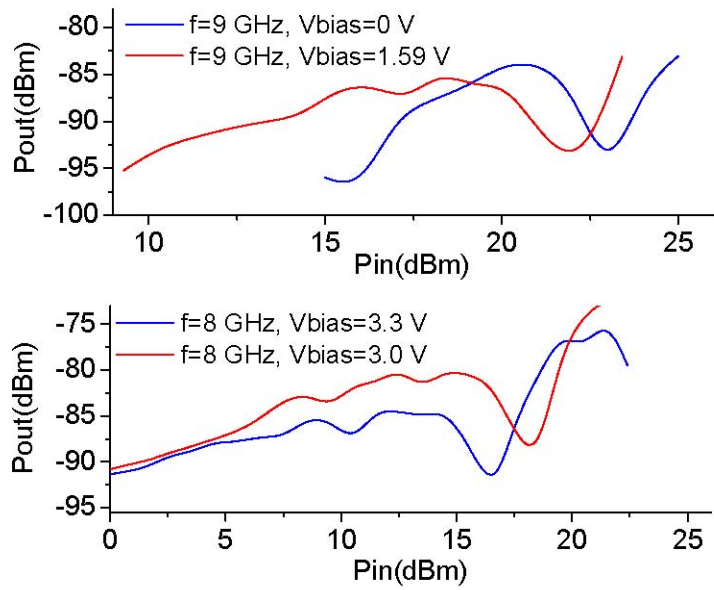
Figure 6: Amplitude transfer functions, T(V), for modulator A2.
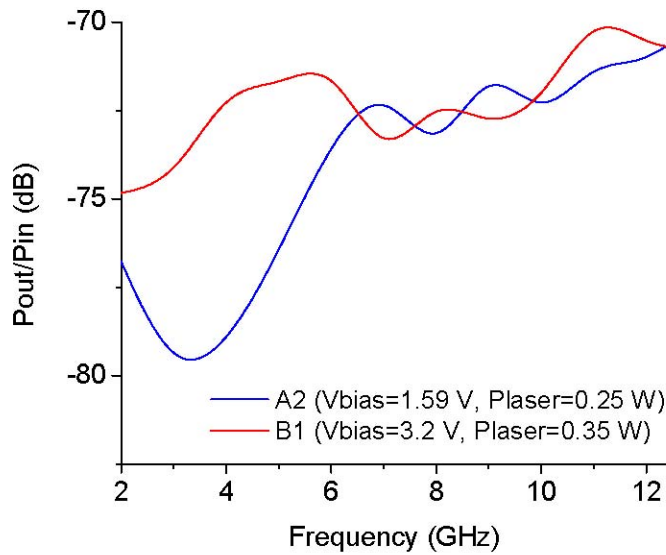
Figure 7: Frequency transfer functions, T(f), for modulators A2 and B1.

The large insertion loss led us to calculate the microstrip impedance of these modulators. For the 25 μm wide trace, with a metallization thickness of 4.5 μm sitting approximately 9 μm above the ground plane and

.

the relative dielectric constant of 2.59210, the characteristic impedance for the microstrip is 35.66 Ohms. The impedance mismatch yields a reflection coefficient of 0.1674 which yields a loss of less than a dB. The microstrip lines are shown in Figure 8.
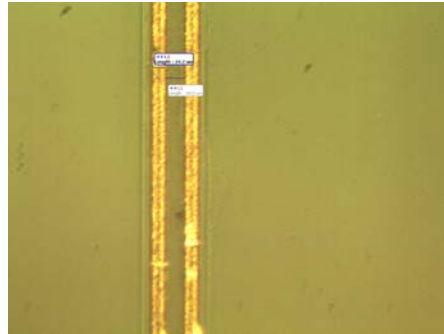

Figure 8: Microstrip modulator electrodes. The traces are 25 μm wide and approximately 4.5 μm thick.